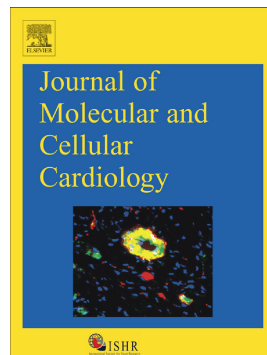


Accepted Manuscript

Myocardial infarction-induced hippocampal microtubule damage by cardiac originating microRNA-1 in mice

Lin-Lin Sun, Ming-Jing Duan, Ji-Chao Ma, Ling Xu, Meng Mao, Das Biddyut, Qin Wang, Chao Yang, Shuai Zhang, Yi Xu, Lin Yang, You Tian, Ying Liu, Sheng-Nan Xia, Ke-Xin Li, Zhuo Jin, Qiaojie Xiong, Jing Ai



PII: S0022-2828(18)30159-7

DOI: [doi:10.1016/j.yjmcc.2018.05.009](https://doi.org/10.1016/j.yjmcc.2018.05.009)

Reference: YJMCC 8737

To appear in: *Journal of Molecular and Cellular Cardiology*

Received date: 24 January 2018

Revised date: 29 April 2018

Accepted date: 12 May 2018

Please cite this article as: Lin-Lin Sun, Ming-Jing Duan, Ji-Chao Ma, Ling Xu, Meng Mao, Das Biddyut, Qin Wang, Chao Yang, Shuai Zhang, Yi Xu, Lin Yang, You Tian, Ying Liu, Sheng-Nan Xia, Ke-Xin Li, Zhuo Jin, Qiaojie Xiong, Jing Ai , Myocardial infarction-induced hippocampal microtubule damage by cardiac originating microRNA-1 in mice. The address for the corresponding author was captured as affiliation for all authors. Please check if appropriate. Yjmcc(2017), doi:[10.1016/j.yjmcc.2018.05.009](https://doi.org/10.1016/j.yjmcc.2018.05.009)

This is a PDF file of an unedited manuscript that has been accepted for publication. As a service to our customers we are providing this early version of the manuscript. The manuscript will undergo copyediting, typesetting, and review of the resulting proof before it is published in its final form. Please note that during the production process errors may be discovered which could affect the content, and all legal disclaimers that apply to the journal pertain.

**Myocardial infarction-induced hippocampal microtubule damage by cardiac originating
microRNA-1 in mice**

Lin-Lin Sun^{a*}, Ming-Jing Duan^{a*}, Ji-Chao Ma^{a*}, Ling Xu^a, Meng Mao^a, Das Biddyut^a, Qin Wang^a, Chao Yang^a, Shuai Zhang^a, Yi Xu^a, Lin Yang^a, You Tian^a, Ying Liu^a, Sheng-Nan Xia^a, Ke-Xin Li^a, Zhuo Jin^a, Qiaojie Xiong^b, Jing Ai^{a\$}

^aDepartment of Pharmacology (The State-Province Key Laboratories of Biomedicine-Pharmaceutics of China), College of Pharmacy of Harbin Medical University, Harbin, Heilongjiang Province, China, 150086

^bDepartment of Neurobiology and Behavior, SUNY at Stony Brook, Stony Brook, NY, USA, 11794

*Lin-Lin Sun, Ming-Jing Duan, Ji-Chao Ma contributed equally to this work.

\$Correspondence to: Jing Ai

E-mail : azhrbmu@126.com

Department of Pharmacology (The State-Province Key Laboratories of Biomedicine-Pharmaceutics of China), College of Pharmacy of Harbin Medical University, Harbin, Heilongjiang Province, China, 150086
P.R. China; Tel.: +86 451 8666-1354; Fax: +86 451 8667-1354.

Abstract

Cardiovascular diseases are risk factors for dementia, but the mechanisms remain elusive. Here, we report that myocardial infarction (MI) generated by the ligation of the left coronary artery (LCA) could lead to increased *miR-1* levels in the hippocampus and blood with neuronal microtubule damage and decreased TPPP/p25 protein expression in the hippocampus. These changes could be prevented by a knockdown of *miR-1* using hippocampal stereotaxic injections of anti-*miR-1* oligonucleotide fragments carried by a lentivirus vector (lenti-pre-AMO-*miR-1*). TPPP/p25 protein was downregulated by *miR-1* overexpression, upregulated by *miR-1* inhibition, and unchanged by binding-site mutations or miR-masks, indicating that the *TPPP/p25* gene was a potential target for *miR-1*. Additionally, the pharmacological inhibition of sphingomyelinase by GW4869 to inhibit exosome generation in the heart significantly attenuated the increased *miR-1* levels in the hippocampi of transgenic (Tg) and MI mice. Collectively, the present study demonstrates that MI could directly lead to neuronal microtubule damage independent of MI-induced chronic brain hypoperfusion but involving the overexpression of *miR-1* in the hippocampus that was transported by exosomes from infarcted hearts. This study reveals a novel insight into the molecular mechanisms of heart-to-brain communication at the miRNA level.

Key words: microRNA-1, myocardial infarction, brain, neuronal microtubule, TPPP/p25, exosome

1. Introduction

In addition to genetic background and ageing, cardiovascular diseases (such as hypertension, atrial fibrillation, or coronary heart disease) are considered to be risk factors for neurodegenerative diseases including cognitive impairments [1-4], which were first described as “cardiogenic dementia” in the late 1970s [5]. Currently, the accepted convention is that various cardiovascular diseases can induce chronic brain hypoperfusion (CBH) by lowering cardiac output and that CBH is responsible for the preclinical condition of mild cognitive impairment (MCI) that is thought to precede dementia [2, 6, 7]. In addition, previous studies have reported that myocardial infarction (MI) induced by the ligation of the left coronary artery (LCA) in rats contributes to forebrain activation by the excessive activity of renin-angiotensin system (RAS) or the secretion of several vasoactive and neuroactive humoral factors [8]. This phenomenon suggests that MI might become a risk factor for abnormal brain function by releasing neurohumoral substances. However, whether there are any other substances released from the infarcted heart that influence brain damage is unknown.

Studies have demonstrated that microRNAs (miRNAs) are not only important regulators of gene expression by targeting mRNAs for cleavage or translational repression in the cell [9, 10] but also biomarkers for multiple-diseases because of their stable existence in various bodily fluids (i.e. serum, plasma, saliva, urine, breast milk, and tears) [11-13]. More strikingly, although several publications data demonstrated that they are expressed in a tissue/cell-specific manner, miRNAs can mediate cell-to-cell communication after being secreted into the extracellular interstitial space from donor cells and accepted by recipient cells with functional targeting capabilities of various transporters [14-16]. These findings prompted us to speculate that abnormal heart function might affect the function of the central nervous system by secreting miRNAs into the blood stream that probably act as neuroactive substances.

MicroRNA-1 (miR-1), a muscle-enriched miRNAs, has been well studied in the regulation of cardiac development [17], arrhythmias [18], and heart failure [19] as well as in apoptosis

[20], and plasma *miR-1* is considered to be a potential biomarker for the prediction of acute myocardial infarction (AMI) [13, 21] and heart failure in patients [22]. Our previous study found that the overexpression of *miR-1* in the transgenic mouse heart induced high expression levels of *miR-1* in the hippocampus and triggered the impaired cognition by the post-transcriptional inhibition of **brain-derived neurotrophic factor (BDNF)** [23]. Considering the relationship between cardiovascular diseases and neurodegenerative diseases [24], we hypothesized that the overexpression of *miR-1* in myocardial infarcted hearts could induce its elevation in the brain, where *miR-1* posttranscriptionally regulates gene expression and controls the neural pathological processes. In this way, *miR-1* mediates heart-disease-to-brain-dysfunction communication.

2. Materials and Methods

2.1. Animals.

Adult male C57BL/6 mice (6-7 months) and SD rats (4-5 months) were used. Animal procedures were approved by the Institutional Animal Care and Use Committee at Harbin Medical University and performed according to the previous experiments guidance[25].

2.2. Synthesis of oligonucleotides.

MiR-1 mimics for rat (sense: 5'-UGGAAUGUAAAGAAGUGUGUAUGU-3'; antisense: 5'-AUACACACUUUCUUUACAUUCCAAU-3') and AMO-*miR-1* (5'-ACCUUACAUUUCUUCACACAUACA-3') were synthesized by Shanghai GenePharma Co., Ltd (Shanghai, China). AMO-1 contains 2'-*O*-methyl modifications. Also a scrambled RNA was used as a negative control (NC) (sense: 5'-UUCUCCGAACGUGUCACGUAA-3' and antisense: 5'-ACGUGACACGUUCGGAGAAUU-3'). The *TPPP*-masking antisense oligodeoxynucleotides (ODNs) were synthesized by Shanghai Sangon Biotech Co., Ltd. *TPPP-ODN-1* was 5'-+A+C+A+TAGGAATGTAATGAA+G+T+G+C-3', which masks the binding sites of *miR-1* located in the position 68-74 of *TPPP/p25* 3'UTR; *TPPP-ODN-2* was 5'-+C+T+T+TCCTGGAATGCTTC+C+T+G+C+-3', which masks the binding sites of

miR-1 located in the position 1880-1886 of *TPPP/p25* 3'UTR. Three nucleotides or deoxynucleotides at both ends of the antisense molecules were locked by a methylene bridge connecting between the 2'-O- and the 4'-C atoms. Locked-nucleic-acid (LNA)-modified oligonucleotides for anti-miR-1 (LNA-anti-miR-1, Methylene Bridge between the 2'-O and the 4'-C atoms) was synthesized by Exiqon (Denmark).

2.3. Mouse model of myocardial infarction.

The method was described by the previous study [18]. The male C57BL/6 mice were used and anesthetized with sodium pentobarbital (40 mg/kg, intraperitoneal). The left anterior descending coronary artery (LCA) was ligated with an 8-0 silk suture and elevated ST segment of electrocardiograph (ECG) was selected as the index to confirm the successful development of myocardial ischaemia. All surgical procedures were performed under sterile condition. After occlusion 3 h, 6 h, 9 h, 1 d, 15 d and 30 d, the hearts, hippocampi and blood were collected for the next experiments.

2.4. Administration of GW4869 into MI and Tg mice.

GW4869 (N,N'Bis[4-(4,5-dihydro-1H-imidazol-2-yl)phenyl]-3,3'-p-phenylene-bis-acrylamide dihydrochloride; MW: 577.5 g/mol; Cayman Chemical) was first dissolved in DMSO solution as the mother liquor with the concentration of 8 mg/mL, which was diluted into the concentration of 0.3 mg/mL by 0.9% NaCl before administration. This study used the method of tail vein injection of GW4869, and the single injection dosage was 200 μ l for each mouse. An equal volume of 3.75% DMSO diluted by 0.9% NaCl was injected into mice as a control group. The first injection was performed on the day before the LCA surgery. After that, GW4869 administration was performed by one time per 2 days for 15 days, and at 24 h after the final injection, mice were sacrificed for the further experiments[26].

2.5. Administration of LNA-modified miR-1 antisense oligonucleotide (LNA-anti*miR-1*) into mice

LNA-anti-miR-1 was delivered into control mice at 4 months of age and age-matched *miR-1* Tg mice through tail vein injection at a dose of 1 mg/kg once every two weeks for eight weeks (ie. 4 injections in two months). Measurements were made 15 days after the last (or the forth) injection when the mice were at an age of 6M [19].

2.6. Permanent, bilateral common carotid artery occlusion (2VO) in the rat.

According to our previous study, bilateral common carotid artery occlusion (2VO) in rats was prepared [27] (www.bio-protocol.org/e2668). Animals were anaesthetized with chloral hydrate (300 mg/kg), and the bilateral common carotid arteries were permanently ligated with 5–0 silk suture. The same procedure was performed on the sham group but without actual ligation. The hippocampus was collected for the measurement of *miR-1* levels from 2VO rats at the time points of 3 h, 6 h, 9 h, 12 h, 1 d, 15 d and 30 d. The extent of cerebral ischemia was evaluated at 3 h, 6 h, 9 h, 12 h, 24h, 15 d and 30 d post 2VO by phosphate-buffered 2% 2,3,5-triphenyltetrazolium chloride (TTC) staining as previous description[27].

2.7. Construction of lentivirus vectors.

To produce *miR-1* antisense inhibitor, two single-stranded DNA oligonucleotides were designed as follows: (1) pre-AMO-*miR-1* (“top strand” oligo: tgctg ATACATACTTCTTACATTCCAGTTGGCCACTGACTGACTGGAATGTAGAAGTAT GTAT) and its complementary sequence (“bottom strand” oligo: cctgATACATACTTCTACATTCCAGTCAGTCAGTGCCAAAATGGAATGTAAAGAA GTATGTATc); (2) negative control (“top strand” oligo: tgctgAAATGTACTGCGCGTGGAGACGTTTGGCCACTGACTGACGTCTCCACGCAG TACATTT) and its complementary sequence (“bottom strand” oligo:

cctgAAATGTACTGCGTGGAGACGTCAGTCAGTGGCCAAAACGTCTCCACGCGCAG TACATTTc). In our previous study we have described the construction of lentivirus vectors [23, 28].

2.8. Stereotactic injection of lentiviral vectors.

After anesthesia, mice were placed onto a stereotaxic frame (RWB Life Science Co. Ltd, China) [23]. Injection coordinates relative to bregma were as follows: AP (anteroposterior), -2.8 mm; ML (mediolateral), ±3.0 mm; DV (dorsoventral), -2.2~2.5 mm below the surface of the dura. A dose of 1.5 µL (10,000 TU/µL) of lenti-pre-AMO-*miR-1* was injected into CA1 region of hippocampus using a 5 µL Hamilton syringe with a 33-gauge tip needle (Hamilton, Bonaduz, Switzerland).

2.9. Evaluation of ultrastructure morphology by transmission electron microscopy.

For transmission electron microscopy detection, mice were anesthetized with sodium pentobarbital (100 mg/kg). Hippocampi were removed and immersed in stationary liquid (pH 7.3) containing 3% glutaraldehyde in 0.1 mmol/L sodium phosphate buffer and 0.45 mmol/L Ca²⁺. Tissue samples were then fixed in 2% Osmic acid (OsO₄) in PBS with 1.5% potassium ferricyanide. After dehydration with a concentration gradient of alcohol solutions, tissues were embedded with propylene oxide as an intermediary solvent. Ultrathin sections were stained with uranyl acetate and lead citrate. Images were examined under a Hitachi H-7650 electron microscope (Hitachi, H-7650, Tokyo, Japan) [29].

2.10. Echocardiography.

The C57BL/6 mice were anesthetized, chest shaved and placed on a temperature maintained heating pad (37°C).ECG and left ventricle ejection fraction (EF) was calculated as previously described [19] .

2.11. Magnetic resonance imaging (MRI) measurements.

Dimeglumine gadopentetate diluted in 0.9% saline was injected once at a dose of 0.06 mmol/kg into the rat's tail vein under anesthesia with chloral hydrate (500 mg/kg,i.p.) The 3.0-T animal MIR scanner (PHILIPS:ACHIEVA 3.0-TX) and animal brain coil were used for MRI measurements.T2-weight image was acquired with the fast spin-echo plus sequences, and the parameters were following: data matrix=100×92, TR=2534ms, effective TE = 40ms, echo train length = 27, field view = 0.8×0.25cm, twenty-five 1-mm slices, and four signal averages. Apparent diffusion coefficient (ADC) values were calculated according to the previous report [30].

2.12. Blood plasma sample preparation.

Whole blood samples (0.5 - 1 mL per mouse) were collected from mice hearts via a direct venous puncture into a vacuum blood collection tube with sodium citrate. A volume of 0.5 mL of whole blood sample was carefully transferred into an RNase-free tube for extraction of RNA[13].

2.13. Evaluation of exosomes.

Plasma exosomes were isolated according to the description of ExoELISA Kit introduction using the ExoQuick precipitation solution (Catalog# EXOQ5A-1). CD63 protein was used as the marker of exosomes in this study and ExoELISA™ kits (System BioSciences, CA, USA) was used according to the manufacturer's instructions. The amount of CD63 proteins were determined by the optical density detected by Infinite 200 PRO multimode reader (Tecan Group Ltd., Germany) at 450 nm [31].

2.14. Primary culture of neonatal rat hippocampal and cortex neurons (NRNs).

Primary hippocampal and cortex neuron cultures were prepared and described by previous study [27] . The hippocampal and cortices were removed from postnatal day 0 (P0) rat pups and the cells were maintained in culture media containing neurobasal medium (Gibco, USA) with 2% B27 supplement (Invitrogen, USA) and 10% of fetal bovine serum (FBS, HyClone,

Logan, UT). The cultures were fed by exchanging 50% of culture media twice a week. Cultures were incubated in a 37 °C humidified atmosphere of 5% CO₂. After 3 days in vitro, the neurons were treated with 5μM cytosine arabinoside (Sigma, USA) to inhibit astrocyte proliferation.

2.15. Primary culture of neonatal rat ventricular cardiomyocytes (NRVCs).

Primary NRVCs were prepared and described by previous study [32]. Cells were isolated from ventricular tissues for 1-3 day-old SD rats and seeded on cover glass in a 6-well plate (2×10⁵/well) in DMEM containing 10% fetal bovine serum (FBS) and 0.1 mmol/L bromodeoxyuridine (sigma) for further experiments. This procedure yielded cultures with 90 ± 5% myocytes, as assessed by microscopic observation of cell beating.

2.16. Co-culture of NRVCs with NRNs.

After 24 h transfection, the cover glasses with cultured NRVCs were taken out from the 6-well plates and gently washed 3 times with PBS. NRNs and NRVCs were indirectly co-cultured at the ratio of 2:1 with the DMEM medium supplemented with 10% fetal bovine serum in two chambers separated by a semi-permeable membrane of Transwell (pore size 0.4 μm) (Cat.# 3412, Corning Company, USA) which allowed for sharing the culture medium, but prevented direct contact between NRVCs and NRNs. NRVCs were cultured in the upper chamber and NRNs in the lower chamber. After 12 h, 24 h or 48 h co-culture, both NRVMs and NRNs were collected for further experiments [33].

2.17. Transfection procedures.

NRVCs or NRNs cultured on cover glasses were washed with an antibiotic-free medium after a 48 h period for adherence and then incubated with 2.0 mL fresh culture medium in 6-well plates without antibiotics. After 24 h, the culture medium was replaced with 2.0 ml fresh serum-free medium without antibiotics. Then, 160 pmol *miR-1* mimics, Cy3 labeled *miR-1* mimics, NC siRNAs or diethyl phosphorocyanidated (DEPC) water was transfected with

X-treme GENE siRNA transfection reagent (Cat.#04476093001, Roche, USA) according to the manufacturer's instructions. Twenty-four hours after transfection, cells on the coverglasses were used for further experiments [19, 27].

2.18. Dual luciferase reporter assay.

To generate reporter vectors bearing miRNA binding sites, we had utilized the full length 3'UTR of mouse *TPPP/p25* genes which were obtained and inserted into multiple sites in the psi-CHECK™-2 luciferase miRNA expression reporter vector (6273 bp, Cat.#C8011, Promega). Luciferase activities were measured with a dual luciferase reporter assay kit (Cat.#E1910, Promega) and a luminometer (GloMax™ 20/20, Promega, USA). Mutagenesis nucleotide-substitution mutations were carried out using direct oligomer synthesis for the 3'UTRs of *TPPP/p25*. All constructs were sequenced verified [19].

2.19 PCR assay

Total RNAs were extracted from NRNs, NRVCs and co-culture medium using Trizol according to the manufacturer's protocol. Reverse transcription of RNA into cDNA was conducted using a ReverTra Ace qPCR RT Kit (Cat.#FSQ101, Toboyo CO., OSAKA, Japan). The primer for reverse transcription of RNA is
“ GTCGTATCCAGTGCCTGTCGTGGAGTCGGCAATTGCACTGGATACGACATACATA C”. The resulting cDNA was used as templates for subsequent PCR amplification using Taq DNA Polymerase (Cat.# P101-01-AB, Vazyme, Nanjing, China). The primers specific for *miR-1* is following: forward: GGC GTGGAATGTAAAGAAG; reverse: TATCCAGTGCCTGTCGTG. S18 was used as an internal control. Then, the amplified products were added into the agarose gel respectively. The parameters of electrophoresis were 100V for 30 min. Images were collected under UV lamp (Tanon 1600, Shanghai, China).

2.20. TaqMan quantitative real-time RT-PCR.

The *miR-1* level was quantified by the TaqMan® MicroRNA Reverse Transcription Kit

(Cat.#4366596, Applied Biosystems) and the TaqMan® Gene Expression Master Mix (for rats: target sequences: UGGAAUGUAAAGAAGUGUGUAU, Cat.#002064; for mouse; UGGAAUGUAAAGAACGUAGUAU, Cat.#002222 Applied Biosystems). We used U6 (Cat.#001973, Applied Biosystems) as an internal control. The PCR protocol was as follows: (1) 95 °C; 10 min, (2) 95 °C; 15 s, 60 °C; 1min (repeat (2) and 40 cycles). The $\delta-\delta$ Ct method was used to calculate the relative expression levels of *miR-1* normalized with U6 [19].

2.21. Pri-miR-1 and Pre-miR-1 assay.

Total RNAs were extracted from hearts and hippocampi of mice using Trizol (Invitrogen) according to the manufacturer's protocol. The reverse transcription primers were 5'-CAAAATACATACTTCTTACATT-3' for pre-mmu-mir-1a-2; 5'-GCAAAGTGGCAGAACAAATGC -3' for pri-mmu-mir-1a-2; and 5'-CGCTTCACGA ATTTGCGTGTCA-3') for mmu-U6. The PCR primers used in this study including : (1) *Pre-miR-1* forward: 5'-TCAGAGCACATACTTCTTATG-3'; and *pre-miR-1* reverse: 5'-CAAAATACATACTTCTTACATT-3'; (2) *Pri- miR-1* forward: 5'-AAGTGTGCATGTGTGAGAGAG-3' and *pri-miR-1* reverse: 5'TCAGTCTGGCGAGAGAGTTC-3'; and (3) U6: forward: 5'-GCTTCGGCAGCACATATACTAAAAT-3', U6 reversed: 5'-CGCTTCACGAATTGCGTGTCA-3'. PCR for *pre-miR-1* was performed under the following condition: 10 min at 95 °C, followed by 15 s at 95 °C, 30 s at 53 °C and 30 s at 72 °C for 40 cycles. PCR for *pri-miR-1* was performed as follows: 10 min at 95°C, followed by 15 s at 95 °C, 30 s at 55 °C and 30 s at 72 °C for 40 cycles. The expression of each *pre-miR-1* related to U6 RNA was determined using the equation $2^{-\Delta C_T}$, where $\Delta C_T = (C_{T\text{miRNA}} - C_{T\text{U6RNA}})$. The final relative gene expression levels were calculated as follows: $2^{-\Delta C_T} \times 10^8$ for *pre-miR-1* and 10^4 for *pri-miR-1* [23, 34].

2.22. Western blot analysis.

Protein samples extracted from the hippocampi of mice or cultured NRNs were used for

immunoblotting analysis described by our previous study [19]. Anti-TPPP/p25 (1:1000, ab92305, Abcam, MA, USA) antibody was used as primary antibody. β -actin (1:1000, G8795, Sigma, Saint Louis, MO, USA) was used as an internal control. Blots were detected with the Odyssey infrared imaging system (Licor, USA). The final results were expressed as fold changes compared with the control values.

2.23. Immunofluorescence detection.

The prepared slices were mounted on glass slides and incubated in PBS containing 10 mg BSA and 2 % Triton X-100 for 1.5 h at room temperature for permeabilization. After blocking by 5% BSA for 1.5 h at room temperature, the primary antibody of CD63 (1:200, ab193349, Abcam, MA, USA) and Anti- β -actin antibody (1:300, ab8227, Abcam, MA, USA) were diluted by PBS with 5% BSA and incubated with slices for 3 days at 4 °C.

For the cultured cells, after 48 h, the co-cultured cardiac myocytes and neurons were fixed in 4% paraformaldehyde for 30 min. After blocking, they were incubated with the primary antibodies anti- β -Tubulin III antibody (Cat.#T8578; 1:200; Sigma, USA) for the neurons, and anti- β -actin antibody (Cat.#ab8227; 1:200; Abcam, MA, USA) for the cardiac myocytes for 3 h at 37°C, and then the cultured cells on the glass were washed and incubated with the secondary antibodies conjugated to Alexa Fluor 488 (Invitrogen) for 1 h at 37°C. After incubation with secondary antibody and DAPI as usual, cardiomyocytes or neurons were mounted on coverslips to obtain confocal images by FluoView™ FV300 (Olympus) using $\times 60$ objective with the same condition at a resolution of 1024 \times 1024 pixels (12 bit).

2.24. Statistical analysis.

Data were described as mean \pm standard error of the mean (s.e.m), and analyzed using one-way ANOVA. The two-tailed Student's t-test was applied for comparisons between two groups. $P < 0.05$ was considered statistically significant. SPSS19.0 was used for all statistical analyses.

3. Results

3.1. Myocardial infarction (MI) contributes to hippocampal microtubules damage.

Hippocampus is an important structure for learning and memory, so we selected the hippocampal CA1 domain to observe whether MI could induce brain damage. The ligation of left anterior descending coronary artery (**LCA**) was selected as the method to develop MI animal model and the elevated ST segment of electrocardiograph (ECG) was used as an index to confirm the successful development of MI model [18] (Figure 1A). To observe whether there was a progressive decrease in heart function during the course of the experiment, ejection fraction (EF) was evaluated and it was significantly decreased at 9 hours after LCA surgery and preserved to 30 days (Figure 1B, n = 5), suggested that LCA surgery could result a persistent low heart function but not a progressive decrease course. Based on this condition, hippocampal samples from MI mice taken 9 h to 30 d after LCA surgery, and a sham group as well, were examined by electron microscopy (EM). We found that the hallmark of changes in the hippocampus was microtubules dissolution that began at 1d and became severe at 30 d (**Figure 1C**, n = 3). Furthermore, the average number of microtubules in each axon largely decreased at 15 d and 30 d after MI compared with LCA surgery time-matched sham mice (**Figure 1 D**, n = 12 axons from 3 mice per group). A previous study has suggested that tubulin polymerization promoting protein (TPPP/p25) plays a major role in maintaining the stability of neuronal microtubules by inducing tubulin polymerization into normal and double-walled microtubules and inducing their bundling[35, 36]; hence we evaluated its expression by western blot. The data showed that the expression of TPPP/p25 protein in the hippocampus was unchanged before 1 d, but decreased on 15 d and 30 d after LCA surgery relative to their time-matched sham mice (**Figure 1E**, n = 6), which corresponded to the damage of neuronal microtubules (**Figure 1, C and D**). These results suggested that a 15 d and 30 d MI, but not transient MI could induce microtubule damage in the hippocampal

region.

3.2. MI increases *miR-1* levels in the hippocampus which targets *TPPP/p25*.

Previous studies have shown that a MI could increase *miR-1* levels in either heart tissue or blood within one day [13, 18, 37]. Therefore, we questioned whether a MI could induce an elevation in *miR-1* levels in the brain in a time-dependent manner and, if so, would that be associated with microtubule dissolution as well as decreased expression of *TPPP/p25*? We found that even though *miR-1* levels were increased in the hippocampal CA1 domain, as assessed by qRT-PCR, the growth began from 1 d to 30 d but not from 3 h to 9 h after LCA surgery (**Figure 2A**, n = 6). As noted earlier, the changes corresponded with the damage of neuronal microtubules (**Figure 1C**) and the altered timeframe of *TPPP/p25* levels in the hippocampus (**Figure 1E**). These results indicated that sustained MIs but not transient MIs could lead to microtubule damage of the hippocampus that might be associated with the downregulation of *TPPP/p25* protein and the overexpression of *miR-1*.

After that we had tried to figure out what was the relationship between the downregulated *TPPP/p25* and increased *miR-1* levels in the hippocampi of mice after a MI? Through a computational analysis of miRNAs using Target scan, microrna.org, and miRDB database, we found that the 3' untranslated region (3'UTR) of *TPPP/p25* had two putative binding sites for *miR-1* (**Figure 2B**). To experimentally verify the *TPPP/p25* gene as a target of *miR-1*, we first cloned the full-length of the 3'UTR of the *TPPP/p25* gene into luciferase-expressing reporter plasmid, and then assessed the effects of *miR-1* on reporter activities in HEK293T cells. The data showed that the co-transfection of *miR-1* with the plasmid consistently produced fewer luciferase activities than the transfection of the plasmid alone. The application of 2'-O-methyl antisense oligoribonucleotides to *miR-1* (AMO-1), a specific inhibitor of *miR-1*, eliminated the suppressive effect of *miR-1* on the *TPPP/p25* gene (**Figure 2C**, n = 3 batches of cells for each group). As shown in **Figure 2D** (n = 3 batches of cells for each group), mutations of the binding sites abolished the effect of *miR-1*, and both

binding sites contributed to the suppressive effects.

Next, we used AMO-1 to determine whether changes in *miR-1* level could affect TPPP/p25 protein expression. *miR-1* or/and AMO-1 were transfected by X-treme GENE siRNA transfection reagent directly into primary cultured neonatal rat hippocampal and cortical neurons (NRNs). Using immunoblotting analysis, we observed that *miR-1* effectively inhibited the expression of TPPP/p25 protein by nearly 60% relative to the control group, whereas the scrambled negative control (NC) of miRNA failed to affect protein levels (**Figure 2E**). In contrast, AMO-1 rescued the downregulation of TPPP/p25 elicited by *miR-1*, indicating the specificity of *miR-1* actions (**Figure 2E**, n = 5 batches of cells for each group). To clarify that the observed changes in TPPP/p25 in cultured NRNs were due to the direct actions of *miR-1* on its binding sites, two miRNA-masking antisense oligodeoxynucleotides (ODNs) fragments (siRNAs) were designed for full base-pairing to *TPPP/p25* at the sequence of motif spanning to mask the binding sites for endogenous *miR-1* with *TPPP/p25* (**Figure 2F**, n = 6 batches of cells for each group), which were labelled *TPPP-ODN-1* and *TPPP-ODN-2* (**Figure 2B**). As expected from their principle modes of action, these miR-masks, unlike AMO-1, did not affect *miR-1* level when co-transfected with *miR-1*. Both *TPPP-ODN-1* and *TPPP-ODN-2* blocked the suppressive effects of *miR-1* on TPPP/p25 protein level (**Figure 2F**). These experiments determined that *miR-1* could regulate the posttranscriptional expression of TPPP/p25 protein by binding at both the 68 - 74 bp and 1880-1888 bp sites of the 3'UTR of the *TPPP/p25* gene.

3.3. Inhibition of miR-1 protects against hippocampal microtubule damage in MI mice.

Next, we predicted that the inhibition of *miR-1* in the hippocampus could block hippocampal microtubule dissolution and prevent the reduction of TPPP/p25 expression in mice suffering from MI. To test this point, anti-*miR-1* oligonucleotide fragments carried by a lentivirus vector (lenti- pre-AMO-*miR-1*) were delivered directly into the hippocampi of mice after the LCA surgery. The data showed that the heart function was significantly decreased after 30 d

of MI which was similar with above data showed in Figure 1B (**Figure 3A**, n = 6), and the *miR-1* levels were significantly increased in the hippocampi of MI mice (**Figure 3B**, n = 6). By comparison, lenti- pre-AMO- *miR-1* effectively blocked the *miR-1* increase in the hippocampus (**Figure 3B**) without affecting the reduced heart functions (**Figure 3A**) or *miR-1* levels in the infarcted hearts (**Figure 3C**). Moreover, lenti-pre-AMO-*miR-1* application prevented microtubules dissolution (**Figure 3D**, n = 3), and the downregulation of TPPP/p25 in the hippocampi of MI mice (**Figure 3E**, n = 6).

3.4. MI increases miR-1 levels in hippocampus through direct heart-brain communication.

Since the reduced cardiac output during MI is associated with changes in cerebral perfusion [6, 38], it was possible that the increasing of *miR-1* levels in the hippocampi of mice observed in our study might have been due to cerebral hypoxia-mediated endogenous biogenesis due to low cardiac output induced chronic brain hypoperfusion (CBH) in MI mice. To address this issue, we established a CBH rat model by permanent bilateral common carotid artery occlusion (2VO) from 3 h to 30 days without MI. We first confirmed cerebral ischemia of 2VO rats by TTC staining. The result showed that the brain ischemia phenotype was onset significantly at 9h and lasted to 30d after 2VO surgery (Figure 4 A), that was similar with our standard for detecting cerebral blood flow (Figure 4 B and C, n = 6). We found that different from MI rats, there was no change of hippocampal microtubules of 2VO rats after surgery 7d to 30d when compared with sham group (Figure 4D). Furthermore, as shown in Figure 4 E (n = 3), *miR-1* levels did not change in the hippocampi of 2VO rats compared with the sham group. Notably, brain ischemia of rats after 2VO surgery from 9h to 30d did not alter the *miR-1* level in the hippocampi relative to 2VO rats without significant brain ischemia after surgery 3 h and 6 h (Figure 4 E), suggesting that brain ischemia alone couldn't induce *miR-1* elevation. These results implied that CBH failed to induce *miR-1* increases as well as microtubules dissolution in the hippocampus. Therefore, we realized that the increased levels of *miR-1* in the hippocampi of MI mice might not be associated with

reduced-cardiac-output-induced CBH. To further exclude the possibility that overexpression of *miR-1* in the hippocampi of MI mice was a result of CBH-induced cerebral hypoxia, we developed an *in vitro* hypoxia model to mimic the hypoxia status (**Figure 4F, left**). We found that, when NRNs alone were treated with 1% O₂ for 48 h, *miR-1* levels were unchanged compared with NRNs which were treated with normal O₂ (**Figure 4F, right**, n = 3 batches of cells for each group), indicating that hypoxia to NRNs alone did not directly upregulate *miR-1* in neurons.

Since mature miRNAs are processed from primary miRNAs (*pri-miRNAs*, long noncoding RNA transcripts containing mature *miRNA* sequences)-generated *pre-miRNAs* (precursors of *miRNAs*) [39], the continued endogenous biogenesis of mature miRNAs should be dependent on a persistent increase in both *pri-miR-1* and *pre-miR-1*. Based on this concept, we detected *pri-miR-1* and *pre-miR-1* in the hippocampi of MI mice. Contrary to our prediction, compared with sham mice, even though both *pri-miR-1* and *pre-miR-1* levels were not increased, they both decreased after 1 d MI instead of remaining unchanged (**Figure 4G and H**, n = 6). To clarify this issue, mature *miR-1* mimics were transfected into NRNs, and we found that the overexpression of mature *miR-1* could feedback inhibit the expression of both *pri-miR-1* and *pre-miR-1* (**Figure 4I**, n = 6 batches of cells for each group). This phenomenon was further circumstantially demonstrated by the decreased expression of *miR-133a*, which shares the same host gene and is controlled by the same promoter (**Figure 4J**, n = 6 batches of cells for each group). Altogether, the data indicated that the elevated *miR-1* levels in the hippocampi of MI mice were not due to endogenous biogenesis.

We then speculated that the increased *miR-1* levels in the hippocampi of MI mice might arise directly from the infarcted heart. If it was true, *miR-1* levels in the heart and blood should be increased after MI. Using qRT-PCR, we found that *miR-1* levels were increased in both the infarcted area and ischaemic border zone of the hearts at 3 h, 6 h, and 9 h time point; however, levels decreased after 1 d of MI (**Figure 4K and L**, n = 6). The timeframe of increased *miR-1* levels in the heart was far ahead of the increase in the hippocampus (**Figure 2A**). Interestingly, compared with sham animals, *miR-1* levels were increased in the blood of

mice from 3 h to 30 d after MI, even though it gradually decreased after 9 h (**Figure 4M**, n = 6). These results indicated the potential for elevating hippocampal *miR-1* levels to have originated from the infarcted heart.

To further intuitively determine if the overexpression of *miR-1* in cardiomyocytes could transfer to neurons, we performed an *in vitro* experiment by developing a cardiomyocyte-neuron co-culture system with the former as a donor and the latter as a recipient. In this NRVCs-NRNs co-culture system (**Figure 5A**), after being transfected with *miR-1* for 24 h, NRVCs were co-cultured with NRNs for 12 h or 24 h. The successful transfection of *miR-1* into NRVCs was first verified by PCR (Figure 5B) and quantified by qRT-PCR (Figure 5C, n = 6 batches of cells for each group). As expected, *miR-1* levels increased significantly in NRNs after 12 h (**Figure 5B & D**, n = 6 batches of cells for each group) of co-culturing and continued to rise at 24h (**Figure 5B & D**), indicating that the overexpressed *miR-1* in the NRVCs might be released into the cell culture medium and subsequently uptaken by NRNs. In addition, this was further confirmed by increased *miR-1* levels in the culture medium confirmed by both PCR and qRT-PCR (**Figure 5E**, n = 10 batches of cells for each group), clearly indicating a release of *miR-1* from NRVCs into the cell culture medium.

Previous studies have reported that miRNAs can be secreted from donor cells and accepted by recipient cells with functional targeting capabilities [10, 15, 33, 40]. If this is true, we should be able to recapitulate this process. First, we had used transwell co-culture system to transfet Cy3-labeled *miR-1* mimics (Cy3-*miR-1*) into NRVCs (**Figure 5F**), and found that *miR-1* could be detected in co-cultured NRNs (**Figure 5G**). Second, severe microtubules dissolutions were also found in NRNs 24 h after co-culture with the *miR-1*-treated NRVCs (**Figure 5H**, n = 3 batches of cells for each group). Third, compared with NC, the protein level of TPPP/p25 in NRNs was significantly reduced 24 h after co-culturing with NRVCs (**Figure 5I**, n = 3 batches of cells for each group), and a similar downregulation of *TPPP/p25* at the mRNA level was observed (**Figure 5J**, n = 3 batches of cells for each group). These data strongly supported the idea that *miR-1* could be transferred from cardiomyocytes to

neurons and induce microtubule damage by inhibiting the expression of the TPPP/p25 protein.

Therefore, to determine if the overexpression of *miR-1* in the heart could actually lead to alterations in hippocampal microtubule and TPPP/p25 protein levels *in vivo*, we used a transgenic (Tg) mouse line with a cardiac-specific overexpression of *miR-1-2* [19]. We first administered the locked nucleic acid-modified *miR-1* antisense inhibitor (LNA-anti-*miR-1*) into mice at the age of 4M to knockdown endogenous *miR-1* via vein injection of four times within two months. As previous reported [19], LNA-anti-*miR-1* efficiently improved the decreased heart function of Tg mice (Figure 6A, n = 6). We also observed that LNA-anti-*miR-1* prevented the increases in *miR-1* levels in the hearts, blood, and hippocampi of Tg mice at the age of 6M (Figure 6B-D). As expected, LNA-anti-*miR-1* mitigated microtubules dissolution in the hippocampus of Tg mice (Figure 6E). Correspondingly, *miR-1*-induced repression of TPPP/p25 was also reversed by LNA-anti-*miR-1* (Figure 6F). Because the hippocampal microtubules damage caused by *miR-1* could be a secondary event due to CBH following depressed cardiac function, the ameliorative hippocampal microtubules damage in hippocampus of LNA-anti-*miR-1* treated Tg mice might be applied to the observed beneficial effects of LNA-anti-*miR-1* against the damaging effects of *miR-1* on the heart. In order to clarify this issue, lenti-pre-AMO-*miR-1* was stereotactically injected directly into the CA1 domain of the bilateral hippocampi of the Tg mice without affecting heart function and brain perfusion of Tg mice. Two months later, we found that lenti-pre-AMO-*miR-1* failed to recover the decreased heart function of Tg mice (Figure 6G, n = 6) and did not inhibit *miR-1* levels in the heart and blood of Tg mice compared with Tg mice that received an injection of a lentiviral vector carrying a negative control fragment (lenti-NC) (Figure 6H and I, n = 6). However, lenti-pre-AMO-*miR-1* significantly inhibited *miR-1* level (>50%) in the hippocampi of Tg mice (Figure 6J, n = 6). As displayed in Figure 6K, although hippocampal microtubule dissolution could be observed, the direct hippocampal application of lenti-AMO-pre-*miR-1* prevented further damage to microtubules compared with age-matched Tg mice and effectively reversed the decrease in TPPP/p25 in the hippocampi of the age-matched Tg mice.

(Figure 6L, n = 6). These data further demonstrate that the overexpression of *miR-1* in the heart directly led to its elevation in the brain and exclude the possibility of CBH as the primary mechanism for the hippocampal microtubule damage in this model.

The next issue was whether cardiac hypoxia or MI also triggers the transport of *miR-1* from the heart to brain. Surprisingly, different than seen from Figure 4F, when NRNs were co-cultured with NRVCs and treated with 1% O₂ together for 48 h (Figure 7A), *miR-1* levels were drastically increased in both NRVCs and NRNs (Figure 7B, n = 6 batches of cells for each group) as well as in the co-culture medium (Figure 7C, n = 10 batches of cells for each group). This phenomenon implied that increased *miR-1* levels in NRNs involved increased *miR-1* levels in NRVCs. To further verify whether the increased *miR-1* in NRNs was from unattached NRVCs, we first treated NRVCs with 1% O₂ alone for 12 h or 24 h first. Interestingly, when hypoxic NRVCs were co-cultured with NRNs, the *miR-1* levels were significantly increased in the co-culture medium (Figure 7D & E, n = 14 batches of cells for each group) and NRNs (Figure 7F, n = 10 batches of cells for each group); however, there was no change in NRVCs (Figure 7F). We then detected the *pri-* and *pre-miR-1* levels of NRVCs. We found that, compared with controls, both the *pri-* and *pre-miR-1* levels were increased in NRVCs following sustained hypoxia (Figure 7G, n = 11 batches of cells for each group). Interestingly, after being co-cultured with NRNs for 24 h, although the *pre-miR-1* was at a high level, the *pri-miR-1* had recovered to regular status; however, not only *pri-* but also *pre-miR-1* levels of NRVCs recovered to control levels after being co-cultured with NRNs for 48 h (Figure 7H, n = 6 batches of cells for each group). These results suggested that sustained hypoxia could induce the biogenesis of *miR-1* in NRVCs continuously, while this process stopped following the termination of the hypoxia intervention. In addition, the decreased *pri-* and *pre-miR-1* levels in co-cultured NRNs further demonstrated that the increased mature *miR-1* in NRNs were not endogenous biogenesis but from the co-cultured pre-hypoxic NRVCs (Figure 7I, n = 6 batches of cells for each group).

3.5. MI induced heart-brain communication involves exosomes.

The next issue was how the heart-originated *miR-1* was transported to the brain. Previous studies have reported that exosomes play a major role in regulating pathophysiological processes including cancer, infectious diseases and neurodegenerative disorders by mediating intercellular communication [41]. Whether exosomes can mediate the long-distance transport of miRNAs from the heart to brain has not been studied so far. To clarify this matter, GW4869 was performed to inhibit sphingomyelinase, which has been reported to inhibit exosome generation [42]. First, we injected GW4869 into the tail vein of *miR-1* Tg mice and found that GW4869 significantly inhibited exosomes biogenesis, as indicated by the decreased green CD63 signal in the cytoplasm of cardiomyocytes compared with Tg mice (**Figure 8A**, n = 3). Further, compared with Tg mice, a supplement of GW4869 also blocked the *miR-1* increasing in the heart (**Figure 8B**, n = 6), blood (**Figure 8C**, n = 6) and hippocampus (**Figure 8D**, n = 6) as well as the reduced expressions of TPPP/p25 protein in the hippocampi of Tg mice (**Figure 8E**, n = 6). Second, we found that MI promoted the biogenesis of exosomes in the ischaemic border zone of the heart, and GW4869 prevented this generation (**Figure 8F**). This phenomenon was further verified by decreased exosome numbers in plasma (**Figure 8G**, n = 6). As predicted, GW4869 treatment effectively prevented MI-induced elevation of *miR-1* levels in the blood (**Figure 8H**, n = 6) and hippocampus (**Figure 8I**, n = 6) and decreased TPPP/p25 protein expressions as well (**Figure 8J**, n = 6). Thus, these results provided sufficient evidence to demonstrate that MI could result in neuronal microtubule damage by *miR-1* overexpression-mediated TPPP/p25 downregulation in an experimental mouse model and that exosomes participated in this pathological process.

4. Discussion

Collectively, the present study demonstrated that MI could directly lead to microtubule damage in hippocampus, which was independent of MI-induced CBH but involved the overexpression of *miR-1* in the hippocampus that were transported by exosomes from the

infarcted heart (**Figure 9**). Thus, our study revealed a novel insight into the potential molecular mechanism of “cardiogenic dementia” at the miRNAs level. Furthermore, based on our results, it is likely that miRNAs can mediate the organ-to-organ communication through the distant release from donor tissue and mimic the action of hormones or neurotransmitters. This phenomenon mainly improves our understanding of the potential for the clinical development of miRNA-based biomarkers and drugs.

4.1. Hippocampal microtubules damage in MI mice involves *miR-1* over-expression-mediated downregulation of *TPPP/p25* protein.

A previous study reported that, although MI mice did not show a spatial memory deficit at 6 weeks after MI, the increased myogenic tone of the proximal cerebral arteries had been developed via tumor necrosis factor- α -dependent activation of sphingosine-1-phosphate signaling [43]. Moreover, MI mice 21 days, but not 3 days displayed upregulation of BACE1 [44]. Furthermore, a very recent study found that a significant impairment in learning in mice at 3 months after MI was accompanied by altered β -amyloid metabolism, apoptosis and inflammation [45]. These investigations indicate that sustained MI, but not transient MI, can induce cerebral abnormalities including changed of inflammation and oxidative stress response, and ultimately leading to impairments in cognition. In the present study, though we did not evaluate the cognitive function and changes of inflammation and oxidative stress, we provided new evidence for that MI in mice from 15 days to 30 days but not within 1 day induces hippocampal microtubules damage, which was similar to other pathological changes in previous reports[43-45]. We then provided solid evidence demonstrated that MI induced hippocampal microtubules damage was mediated by the overexpression of *miR-1* in the hippocampus. First, the onset of hippocampal microtubules injury corresponded well with the time-course of *miR-1* increases in the hippocampi of mice during MI. Second, the overexpression of *miR-1* in NRVCs induced microtubule dissolution in co-cultured NRNs, which was consistent with the hippocampal microtubules damage induced by MI in mice. Third, in *miR-1* Tg mice, we found detrimental microtubules remodeling similar to that

observed in the hippocampi of MI mice and co-cultured NRNs. Importantly, the microtubules damage could be alleviated by stereotaxic hippocampal injection of lenti-pre-AMO-*miR-1*.

Fourth, following the stereotaxic injection of lenti-pre-AMO-*miR-1* into the hippocampi of mice with MI, the MI-mediated hippocampal microtubule damage was alleviated while the decreased heart function was not recovered. Finally, as we know, inflammation and oxidative stress could results multiple pathological changes that might involve microtubule damage, and brain ischeamia is the direct inducer of inflammation and oxidative stress responses. Here we found that, although CBH induced by 2VO surgery 30 days resulted marked increase of autophagic vacuoles [29], however, the microtubule morphology was unaltered. All of these data indicated that MI-mediated hippocampal microtubule damage was associated with increased *miR-1* levels in the hippocampus. Notably, in the present study, we focused on hippocampus because it is an important region of brain involved in declarative learning and memory. We cannot exclude the damaging effects of *miR-1* on other brain regions, which needs to be clarified in the future. In addition, we found that the significant increased *miR-1* levels and reduced TPPP/p25 protein expression of hippocampus was presented at 15 days but not at within 1 day after LCA surgery. The results indicated again that was sustained MI but not transient MI can induce abnormal pathology changes in the brain and provide insight into heart diseases could induce brain damages. The phenomena may due to the time spent during the transportation in the circulation as well as the acceptance and accumulation by neurons.

Previous studies have demonstrated that TPPP/p25 promotes the polymerization of tubulin into double-walled tubules and polymorphic aggregates [35], plays a central role in the stabilization of the microtubule network[46], and is considered to be a potential drug target for Parkinson's disease[47]. Here, we found that the expression of TPPP/p25 was decreased in the hippocampi of mice after 15 days and 30 days MI, which matched the timeframe of altered *miR-1* levels. Furthermore, we found that *TPPP/p25* gene was the target for *miR-1* which was demonstrated by a series of experiments including a dual luciferase reporter assay and the transfection of *miR-1* mimics, AMO-1 and miR-masking ODNs into

primary cultured neurons. Note that, similar to previous study[48], anti-miR-1 by intravenous injection of LNA-anti-*miR-1* effectively prevented the increases in *miR-1* levels in the hearts, blood, and hippocampi of Tg mice, as well as the microtubules dissolution. Since LNA-anti-*miR-1* also improved the decreased heart function of Tg mice, the ameliorative hippocampal microtubules damage in hippocampus of LNA-anti-*miR-1* treated Tg mice might be due to beneficial effects of LNA-anti-*miR-1* against the damaging effects of *miR-1* on the heart. We then performed the hippocampal stereotaxic injection of lenti-pre-AMO-*miR-1* and found that lenti-pre-AMO-*miR-1* could prevent decreased TPPP/p25 expression accompanied by a reduction in *miR-1* levels in the hippocampi of cardiac-*miR-1* overexpression Tg mice. Importantly, the reduction in *miR-1* induced by hippocampal stereotaxic injection of lenti-pre-AMO-*miR-1* significantly attenuated the TPPP/p25 decrease in the hippocampi of MI mice without affecting CBH.

Obviously, as one kind of miRNAs, *miR-1* also has multiple-targets which mean the overexpression of *miR-1* in the brain would lead to various pathological changes by targeting various genes. For example, our previous study reported that *miR-1* could posttranscriptional downregulate BDNF expression [23], which mentioned a close relationship with synaptic plasticity. In this study, we provided evidence that the overexpression of *miR-1* in the hippocampus could lead to hippocampal microtubule dissolution by targeting the *TPPP/p25* gene. While, what extent changes in TPPP/p25 in the hippocampus could explain the cognitive changes needs further studied. Furthermore, since TPPP/p25 also had a high expression in glial cells, we believe that the damaging effect of *miR-1* on hippocampal microtubules was non-neuronal specific.

4.2. *MiR-1 increases in the hippocampi of MI mice involves exosomes*

As we know, *miR-1* is a muscle-enriched miRNA that is highly expressed in the heart but has a very low expression level in the brain. So as apparent issue was that the increased *miR-1* in the hippocampus comes from where? There were two possibilities. The first possibility was

that *miR-1* expression was endogenous biogenesis in the brain as a result of CBH due to sustained MI-induced low cardiac output. To clarify this issue, an animal model of 2VO was established according to previous studies [27]; Here we used SD rat but not mouse to perform 2VO surgery is because the Willis circle of mouse is too small to make mouse alive more than 3 days. Different from previous study that reported *miR-1* increased in N2a cell line, which is mouse neuroblastoma cell line, following oxygen/glucose deprivation (OGD)[49], our results showed that 2VO caused obvious CBH, but failed to induce any increase in *miR-1* expression in the hippocampus. Specifically, in the present study we found that the brain ischemia phenotype was onset significantly at 9 hours and lasted to 30 days but not began from 3 hours after 2VO surgery. Interestingly, the *miR-1* levels were not changed among these rats. That means brain ischeamia of rats after 2VO surgery from 9 hours to 30 days did not alter the *miR-1* level in the hippocampi relative to 2VO rats without significant brain ischeamia after surgery 3 hours and 6 hours. Similarly, we found that there was no change of *miR-1* level in the hippocampi of MI mice at 9 h after surgery although it has displayed a significantly decreased heart function that is a theoretical inducer of brain hypoperfusion due to peri-procedural hypotension. Also, in this study, when NRNs alone were treated with 1% O₂, the *miR-1* levels did not change compared with the control group. This disparity may due to different cell type and/or different hypoxia strategy. However, when NRNs were co-cultured with NRVCs, hypoxia remarkably increased *miR-1* levels in both NRVCs and NRNs. This phenomenon indicated that increased *miR-1* levels in NRNs were dependent on hypoxic NRVCs but not neuronal hypoxia alone. Particularly, not increased *pri-* or *pre-miR-1* levels in the hippocampi of MI mice and/or hypoxic NRNs *in vitro* further excluded the possibility of the endogenous biogenesis of *miR-1* in the MI mouse brain. The second possible explanation for the increased *miR-1* in the hippocampus was originated from the exogenous *miR-1* of infarcted cardiac tissues which then released into the blood and delivered to the brain where hippocampal neurons subsequently absorbed it. To clarify this issue, we first compared *miR-1* levels between hippocampus and the heart. We found that *miR-1* levels were

increased in the heart far before they increased in the hippocampus; *miR-1* levels were increased in the blood of mice from 3 h to 30 d after MI. This phenomenon hinted a potency of elevating hippocampal *miR-1* levels might have potentially originated from the infarcted heart. Second, we developed a cardiomyocyte-neuron co-culture system to perform several *in vitro* experiments, and demonstrated that the overexpression of *miR-1* in NRVCs could lead to *miR-1* increases in co-cultured un-attached NRNs, indicating the possibility of *miR-1* transfer from cardiomyocytes to neurons. Exosomes function in the transport of mRNAs, miRNAs and proteins and it can cross the blood-brain barrier [50]. Recently, studies have demonstrated that exosomes from cardiomyocytes can transfet other cell types [51], and they were considered prominent mediators of neurodegenerative diseases [50]. In the present study, we observed that the pharmacological inhibition of sphingomyelinase by GW4869 to inhibit exosomes generation in the heart could block the increases in *miR-1* levels in the blood and hippocampus and prevented the reduced expression of the TPPP/p25 protein in the hippocampi of both Tg and MI mice.

It is worth noting that exosomes have been found to contain up to 121 miRNAs, including *miR-1*, *miR-15*, *miR-16*, *miR-17*, *miR-18*, *miR-181*, *miR-375*, *lin-4* and *let-7* [52], and previous studies have demonstrated that MI could induce different miRNAs changes such as in *miR-1*[18]. This phenomenon suggests that MI-induced brain damage might be associated with all of these altered miRNAs when they were transported into the brain. However, in the present study, we demonstrated that hippocampal microtubule damage in MI mice was due to the overexpression of *miR-1* in the hippocampus. Moreover, since sphingomyelinase was not the specific for exosome biogenesis, the application of GW4869 would affect the generation of all vesicles that might also associated with miRNA transportation. In the present study, we used CD63 as a marker of exosomes and demonstrated that exosome biogenesis was decreased in the MI heart and its level also reduced in the blood. Taken together, these results suggested that MI-induced overexpression of *miR-1* in the brain might involve exosomes that were released from the heart and entered into the brain where they are absorbed by hippocampal neurons.

The present study provided important information that the persistently high level of *miR-1* in the blood of patients with MI might have the potential to be a biomarker for the onset of cognitive impairments that might precede the onset of heart failure. However, whether *miR-1* can induce other pathological changes in the hippocampi of mice with MI via the direct or indirect regulation of other potential target genes and the molecular mechanism of MI procedure induced brain anoxic injury needs to be elucidated further.

Collectively, the provocative finding from the present study is that MI alone could promote brain damage, which was mediated by the heart-originating overexpression of *miR-1* in the hippocampus. Thus, we first reported for the first time that miRNAs can mediate communication between distal tissues in addition to mediating nearby cell-to-cell communication, and serve as a link between different pathological processes. Our study also reveals a new aspect of the biological function of miRNAs and provides a new strategy for the use of miRNA interference in the treatment of diseases.

Acknowledgements

This work was supported by Natural Science Foundation of China (81671052, 81471115, and 81271207 to Jing Ai) and the Scientific Research Innovation Fund of Harbin Medical University (YJSCX2015-12HYD to L.L.S, and YJSCX2016-12HYD to M.L.Y).

Author Contributions

JA designed and supervised the manuscript. LS, MD, LX, JM, MM, QW, CY, SZ, YX, LY, YT, YL, SX, KL and ZJ performed the experiments. JA performed the statistical analyses. JA, D. Biddyut and QX wrote the manuscript.

Potential Conflicts of Interest

Nothing to report

References

- [1] de Toledo Ferraz Alves TC, Ferreira LK, Wajngarten M, Busatto GF. Cardiac disorders as risk factors for Alzheimer's disease. *J Alzheimers Dis.* 2010;20:749-63.
- [2] MonsuezJJ, Gesquiere-Dando A, Rivera S. Cardiovascular prevention of cognitive decline. *Cardiol Res Pract.* 2011;2011:250970.
- [3] Jefferson AL, Beiser AS, Himali JJ, Seshadri S, O'Donnell CJ, Manning WJ, et al. Low cardiac index is associated with incident dementia and Alzheimer disease: the Framingham Heart Study. *Circulation.* 2015;131:1333-9.
- [4] Jacobs V, Cutler MJ, Day JD, Bunch TJ. Atrial fibrillation and dementia. *Trends Cardiovasc Med.* 2015;25:44-51.
- [5] Cardiogenic Dementia. *Lancet.* 1977;1:27-8.
- [6] Jefferson AL. Cardiac output as a potential risk factor for abnormal brain aging. *J Alzheimers Dis.* 2010;20:813-21.
- [7] de la Torre JC. Cardiovascular risk factors promote brain hypoperfusion leading to cognitive decline and dementia. *Cardiovascular psychiatry and neurology.* 2012;2012:367516.
- [8] Francis GS. Neurohumoral activation and progression of heart failure: hypothetical and clinical considerations. *J Cardiovasc Pharmacol.* 1998;32 Suppl 1:S16-21.
- [9] Ebert MS, Sharp PA. Roles for microRNAs in conferring robustness to biological processes. *Cell.* 2012;149:515-24.
- [10] Montecalvo A, Larregina AT, Shufesky WJ, Stoltz DB, Sullivan ML, Karlsson JM, et al. Mechanism of transfer of functional microRNAs between mouse dendritic cells via exosomes. *Blood.* 2012;119:756-66.
- [11] Cortez MA, Bueso-Ramos C, Ferdin J, Lopez-Berestein G, Sood AK, Calin GA. MicroRNAs in body fluids--the mix of hormones and biomarkers. *Nat Rev Clin Oncol.* 2011;8:467-77.
- [12] Chen X, Liang H, Zhang J, Zen K, Zhang CY. Secreted microRNAs: a new form of intercellular communication. *Trends Cell Biol.* 2012;22:125-32.
- [13] Ai J, Zhang R, Li Y, Pu J, Lu Y, Jiao J, et al. Circulating microRNA-1 as a potential novel biomarker for acute myocardial infarction. *Biochem Biophys Res Commun.* 2010;391:73-7.
- [14] Redis RS, Calin S, Yang Y, You MJ, Calin GA. Cell-to-cell miRNA transfer: from body homeostasis to therapy. *Pharmacol Ther.* 2012;136:169-74.
- [15] Vickers KC, Palmisano BT, Shoucri BM, Shamburek RD, Remaley AT. MicroRNAs are transported in plasma and delivered to recipient cells by high-density lipoproteins. *Nat Cell Biol.* 2011;13:423-33.
- [16] Raji GR, Sruthi TV, Edatt L, Haritha K, Sharath Shankar S, Sameer Kumar VB. Horizontal transfer of miR-106a/b from cisplatin resistant hepatocarcinoma cells can alter the sensitivity of cervical cancer cells to cisplatin. *Cell Signal.* 2017;38:146-58.
- [17] Zhao Y, Samal E, Srivastava D. Serum response factor regulates a muscle-specific microRNA that targets Hand2 during cardiogenesis. *Nature.* 2005;436:214-20.
- [18] Yang B, Lin H, Xiao J, Lu Y, Luo X, Li B, et al. The muscle-specific microRNA miR-1 regulates cardiac arrhythmogenic potential by targeting GJA1 and KCNJ2. *Nat Med.* 2007;13:486-91.
- [19] Ai J, Zhang R, Gao X, Niu HF, Wang N, Xu Y, et al. Overexpression of microRNA-1 impairs cardiac contractile function by damaging sarcomere assembly. *Cardiovasc Res.* 2012;95:385-93.
- [20] Tang Y, Zheng J, Sun Y, Wu Z, Liu Z, Huang G. MicroRNA-1 regulates cardiomyocyte apoptosis by targeting Bcl-2. *Int Heart J.* 2009;50:377-87.

- [21] Cheng Y, Tan N, Yang J, Liu X, Cao X, He P, et al. A translational study of circulating cell-free microRNA-1 in acute myocardial infarction. *Clin Sci (Lond)*. 2010.
- [22] Tijesen AJ, Creemers EE, Moerland PD, de Windt LJ, van der Wal AC, Kok WE, et al. MiR423-5p as a circulating biomarker for heart failure. *Circ Res*. 2010;106:1035-9.
- [23] Ma JC, Duan MJ, Sun LL, Yan ML, Liu T, Wang Q, et al. Cardiac over-expression of microRNA-1 induces impairment of cognition in mice. *Neuroscience*. 2015;299:66-78.
- [24] Bhat NR. Linking cardiometabolic disorders to sporadic Alzheimer's disease: a perspective on potential mechanisms and mediators. *J Neurochem*. 2010;115:551-62.
- [25] Kilkenny C, Browne WJ, Cuthill IC, Emerson M, Altman DG. Improving bioscience research reporting: the ARRIVE guidelines for reporting animal research. *PLoS Biol*. 2010;8:e1000412.
- [26] Iguchi Y, Eid L, Parent M, Soucy G, Bareil C, Riku Y, et al. Exosome secretion is a key pathway for clearance of pathological TDP-43. *Brain*. 2016;139:3187-201.
- [27] Ai J, Sun LH, Che H, Zhang R, Zhang TZ, Wu WC, et al. MicroRNA-195 protects against dementia induced by chronic brain hypoperfusion via its anti-amyloidogenic effect in rats. *J Neurosci*. 2013;33:3989-4001.
- [28] Sun LH, Yan ML, Hu XL, Peng LW, Che H, Bao YN, et al. MicroRNA-9 induces defective trafficking of Nav1.1 and Nav1.2 by targeting Navbeta2 protein coding region in rat with chronic brain hypoperfusion. *Molecular neurodegeneration*. 2015;10:36.
- [29] Che H, Yan Y, Kang XH, Guo F, Yan ML, Liu HL, et al. MicroRNA-27a Promotes Inefficient Lysosomal Clearance in the Hippocampi of Rats Following Chronic Brain Hypoperfusion. *Mol Neurobiol*. 2017;54:2595-610.
- [30] Wang S, Wu EX, Tam CN, Lau HF, Cheung PT, Khong PL. Characterization of white matter injury in a hypoxic-ischemic neonatal rat model by diffusion tensor MRI. *Stroke*. 2008;39:2348-53.
- [31] Dubovsky JA, Chappell DL, Harrington BK, Agrawal K, Andritsos LA, Flynn JM, et al. Lymphocyte cytosolic protein 1 is a chronic lymphocytic leukemia membrane-associated antigen critical to niche homing. *Blood*. 2013;122:3308-16.
- [32] Sun LY, Wang N, Ban T, Sun YH, Han Y, Sun LL, et al. MicroRNA-23a mediates mitochondrial compromise in estrogen deficiency-induced concentric remodeling via targeting PGC-1alpha. *J Mol Cell Cardiol*. 2014;75:1-11.
- [33] Hergenreider E, Heydt S, Treguer K, Boettger T, Horrevoets AJ, Zeiher AM, et al. Atheroprotective communication between endothelial cells and smooth muscle cells through miRNAs. *Nat Cell Biol*. 2012;14:249-56.
- [34] Schmittgen TD, Jiang J, Liu Q, Yang L. A high-throughput method to monitor the expression of microRNA precursors. *Nucleic Acids Res*. 2004;32:e43.
- [35] Tirian L, Hlavanda E, Olah J, Horvath I, Orosz F, Szabo B, et al. TPPP/p25 promotes tubulin assemblies and blocks mitotic spindle formation. *Proc Natl Acad Sci U S A*. 2003;100:13976-81.
- [36] Ovadi J. The tubulin polymerization promoting protein, TPPP/p25. *IUBMB Life*. 2008;60:637-42.
- [37] Bostjancic E, Zidar N, Stajner D, Glavac D. MicroRNA miR-1 is up-regulated in remote myocardium in patients with myocardial infarction. *Folia biologica*. 2010;56:27-31.
- [38] Felder RB, Francis J, Zhang ZH, Wei SG, Weiss RM, Johnson AK. Heart failure and the brain: new perspectives. *Am J Physiol Regul Integr Comp Physiol*. 2003;284:R259-76.
- [39] Winter J, Jung S, Keller S, Gregory RI, Diederichs S. Many roads to maturity: microRNA biogenesis pathways and their regulation. *Nat Cell Biol*. 2009;11:228-34.
- [40] Stoorvogel W. Functional transfer of microRNA by exosomes. *Blood*. 2012;119:646-8.

- [41] S ELA, Mager I, Breakefield XO, Wood MJ. Extracellular vesicles: biology and emerging therapeutic opportunities. *Nat Rev Drug Discov.* 2013;12:347-57.
- [42] Kosaka N, Iguchi H, Yoshioka Y, Takeshita F, Matsuki Y, Ochiya T. Secretory mechanisms and intercellular transfer of microRNAs in living cells. *J Biol Chem.* 2010;285:17442-52.
- [43] Yang J, Noyan-Ashraf MH, Meissner A, Voigtlaender-Bolz J, Kroetsch JT, Foltz W, et al. Proximal cerebral arteries develop myogenic responsiveness in heart failure via tumor necrosis factor-alpha-dependent activation of sphingosine-1-phosphate signaling. *Circulation.* 2012;126:196-206.
- [44] Nural-Guvener HF, Muthu N, Gaballa MA. BACE1 levels are elevated in congestive heart failure. *Neurosci Lett.* 2013;532:7-11.
- [45] Hong X, Bu L, Wang Y, Xu J, Wu J, Huang Y, et al. Increases in the risk of cognitive impairment and alterations of cerebral beta-amyloid metabolism in mouse model of heart failure. *PLoS One.* 2013;8:e63829.
- [46] Vincze O, Tokesi N, Olah J, Hlavanda E, Zotter A, Horvath I, et al. Tubulin polymerization promoting proteins (TPPPs): members of a new family with distinct structures and functions. *Biochemistry.* 2006;45:13818-26.
- [47] Olah J, Ovadi J. Dual life of TPPP/p25 evolved in physiological and pathological conditions. *Biochem Soc Trans.* 2014;42:1762-7.
- [48] Selvamani A, Sohrabji F. Mir363-3p improves ischemic stroke outcomes in female but not male rats. *Neurochem Int.* 2017;107:168-81.
- [49] Chang CY, Lui TN, Lin JW, Lin YL, Hsing CH, Wang JJ, et al. Roles of microRNA-1 in hypoxia-induced apoptotic insults to neuronal cells. *Arch Toxicol.* 2016;90:191-202.
- [50] Tsilioni I, Panagiotidou S, Theoharides TC. Exosomes in neurologic and psychiatric disorders. *Clin Ther.* 2014;36:882-8.
- [51] Waldenstrom A, Ronquist G. Role of exosomes in myocardial remodeling. *Circ Res.* 2014;114:315-24.
- [52] Lotvall J, Valadi H. Cell to cell signalling via exosomes through esRNA. *Cell Adh Migr.* 2007;1:156-8.

Figure legends

Figure 1. Myocardial infarction (MI) induced by LCA surgery be gets hippocampal microtubules damage. (A) Development of MI mice model confirmed by elevated ST segment. (B) Significantly decreased ejection fraction (EF %) in MI mice from 9 hours to 30 days after LCA surgery. Mean \pm s.e.m, n = 5, *P < 0.05. (C) Morphological characterization of hippocampal microtubules in mice after LCA surgery examined by electron microscopy (EM). n = 3 animals per group, scale: 1 μ m. (D) Quantitative analysis of the number of microtubules. Mean \pm s.e.m, n = 12 axons from 3 animals per group, *P < 0.05 vs sham group. (E) Expression of TPPP/p25 protein in the hippocampi of mice at different time points after LCA surgery. Mean \pm s.e.m, n = 6, *P < 0.05 vs sham group.

Figure 2. MI increases miR-1 level in the hippocampus which targets TPPP/p25. (A) miR-1 expression measured by qRT-PCR in the hippocampi from MI mice induced by LCA surgery at different time points. Mean \pm s.e.m, n = 6, *P < 0.05 vs sham group. (B) Complementarity between miR-1 seed sequence (5'end 2-8 nucleotides) and the 3'UTR of the mouse's TPPP/p25. Watson-Crick complementarity is connected by “|”. The underlines indicate nucleotide replacement mutations to the genes. The miRNA-masking antisense oligodeoxynucleotides (ODNs) are in blue font. (C, D) Luciferase reporter gene assay for interactions between miR-1 and its binding sites (C) or mutated binding sites (D) in the 3'UTR of the TPPP/p25 mRNA in HEK293T cells. n = 3, *P < 0.05 vs blank, [#]P < 0.05 vs miR-1. (E) miR-1 inhibits the expression of TPPP/p25 in primary cultured NRNs. Upper panel: action mode of AMO-1 with miR-1. The high-binding affinity of AMO-1 leads to the functional inhibition of miR-1, leading to the derepression of target mRNAs. ORF: open reading frame; AGO: Argonaut. Lower panel: Effects of miR-1 on the protein level of endogenous TPPP/p25 in primary cultured NRNs as determined by western blot analysis. Cells were transfected with miR-1, AMO-1, miR-1+AMO-1, or NC. n = 5 batches of cells for each group. *P < 0.05 vs NC; [#]P < 0.05 vs miR-1. (F) TPPP-ODNs block the action of miR-1 on TPPP/p25 expression. Upper panel: action mode of miR-mask ODNs. Gene-specific ODNs (designed as 22

oligonucleotides fully complementary to the complete sequence of *miR-1* target sites in the 3'UTRs of target mRNAs) with high binding affinity completely masked the target sites of *miR-1* in the 3'UTRs of target mRNAs, which block the suppression of target mRNAs. Lower panel: De-repression of TPPP/p25 by *TPPP-ODNs* as determined by western blot analysis. *n* = 6 batches of cells for each group. **P* < 0.05 vs NC; #*P* < 0.05 vs *miR-1*.

Figure 3. Downregulation of hippocampal *miR-1* prevents hippocampal microtubule dissolution and restores TPPP/p25 expression in MI mice induced by LCA surgery. (A)

Stereotaxic injection of lenti-pre-AMO-*miR-1* into the hippocampus did not affect the decreased ejection fraction (EF %) in LCA surgery mice. Mean ± s.e.m, *n* = 6, **P* < 0.05. (B,C) *miR-1* levels in the hippocampi (B) and hearts (C) of LCA mice after stereotaxic injection of lenti-pre-AMO-*miR-1* into the CA1 domain of the hippocampus as measured by qRT-PCR. Mean ± s.e.m, *n* = 6 animals per group, **P* < 0.05 vs WT group, #*P* < 0.05 vs LCA+NC. (D) Stereotaxic injection of lenti-AMO-pre-*miR-1* into the hippocampus prevents hippocampal microtubule dissolution in LCA mice as seen by EM. Scale bar: 2 μm for the up panel and 4 μm for the lower panel. (E) Stereotaxic injection of lenti-AMO-pre-*miR-1* into the hippocampus upregulates the expression of TPPP/p25 protein in LCA mice as evaluated by western blot. **P* < 0.05 vs WT; #*P* < 0.05 vs MI+NC; means ± s.e.m, *n* = 6 animals per group.

Figure 4. MI increases *miR-1* levels in the hippocampus independent of CBH. (A)

Characterization of cerebral ischemia in a coronal section after 2VO for 3h, 6h, 9h, 12h, 24h, 15d and 30d. TTC staining was used to identify the brain ischemia. Red represents normal tissue and white represents infarct tissue. (B) fMRI analysis of cortex and medulla in rats at 30 d after 2VO. The left images on the left show decreased brain blood flow indicated by blue colour. MRI, magnetic resonance imaging. (C) Quantitative analysis of ADC values in rat brains. ADC, apparent diffusion coefficient. Mean ± s.e.m, *n* = 6 animals per group. (D) Morphological characterization of hippocampal microtubules in rats after 2VO

surgery examined by electron microscopy (EM). n = 3 animals per group, scale: 1 μ m. (E)

miR-1 levels in the hippocampi of rats following 2VO at different time points. Mean \pm s.e.m, n = 3 animals per group. (F) Neuronal hypoxia does not elevate *miR-1* levels. Left: experimental design; right: *miR-1* level in NRNs. n = 3 batches of cells for each group. *P < 0.05 vs Ctl. (G-H) The expressions of *pri-miR-1* (G) and *pre-miR-1* (H) in the hippocampi of mice after LCA surgery at different time points. Mean \pm s.e.m, n = 6 animals per group, *P<0.05 vs sham group. (I) Overexpression of *miR-1* inhibits the expression of *pri-* and *pre-miR-1* in primary cultured NRNs. n = 6 batches of cells for each group. *P < 0.05 vs NC. (J) Overexpression of *miR-1* inhibits the expression of *miR-133a* in primary cultured NRNs. n = 6 batches of cells for each group. *P < 0.05 vs NC. (K-M) The expression of *miR-1* in the infarcted area (K) and ischaemic border zone (L) of the heart, as well as the blood (M) from mice after LCA surgery at different time points. Mean \pm s.e.m, n = 6 animals per group, * P< 0.05 vs sham group.

Figure 5 Overexpression of *miR-1* in NRVCs damages the microtubules of co-cultured NRNs. (A) Experimental design. NRVCs were cultured on cover glasses within a 6-well dish. A total 160 pmol of *miR-1* and NC siRNAs or diethyl phosphorocyanide (DEPC) water were transfected into NRVCs with X-treme GENE siRNA transfection reagent for 24 h. Then an *in vitro* co-culture system was used where NRVCs were seeded in the top compartment, and NRNs were cultured in the bottom compartment. A membrane with a 0.4- μ m pore size separated the two compartments to prevent NRVCs from directly connecting to NRNs. NRNs were co-cultured with NRVCs for 12 or 24 h for subsequent experiments. (B) *miR-1* levels in NRVCs and NRNs after co-culture 12 h or 24 h, as measured by PCR. (C-D) *miR-1* levels in NRVCs (C), NRNs (D) after co-culture 12 h or 24 h, as measured by qRT-PCR. Mean \pm s.e.m, n = 6 batches for NRVCs and NRNs, *P < 0.05 vs NC. (E) *miR-1* levels in culture medium after co-culture 24 h, as measured by qRT-PCR and PCR (inserted image), Mean \pm s.e.m, n = 10 batches. (F) Transfection of Cy3 labelled *miR-1* mimics (*Cy3-miR-1*) by X-treme in to NRVCs. Upper panel: transfection of NC into NRVCs by X-treme without labelling of Cy3.

Bottom: transfection of *miR-1* mimics into NRVCs by X-treme with labelling of Cy3. Blue: DAPI; Red: Cy3-*miR-1*; Green: β-actin. Scale bar: 20 μm. (G) The transfer of Cy3-*miR-1* from NRVCs to co-cultured NRNs. Upper panel: NRNs co-cultured with NRVCs transfected with NC without labelling of Cy3; Bottom: NRNs co-cultured with NRVCs transfected with Cy3 labelled *miR-1* mimics. Blue: DAPI; Red: Cy3-*miR-1*; Green: β-Tubulin III. (H) *miR-1* transfection into NRVCs induces NRNs microtubule dissolution at 24 h after the initiation of co-culture. $n = 3$ batches of cells for each group, scale bar: 20 μm. (I, J) Overexpression of *miR-1* in NRVCs inhibits the expression of TPPP/p25 in NRNs 24 h after co-culture at both the protein (H) and mRNA (I) levels. $n = 3$ batches of cells for each group. * $P < 0.05$ vs NC.

Figure 6. Inhibition of *miR-1* prevents hippocampal microtubule dissolution in Tg mice.

(A) Intravenous injection of LNA-anti-*miR-1* (LNA-1) improved the decreased ejection fraction (EF %) in Tg mice. Mean ± s.e.m, $n = 6$, * $P < 0.05$. (B-D) LNA-anti-*miR-1* treatment prevented the increased *miR-1* levels in the heart (B), blood (C) and hippocampus (D) in *miR-1* Tg mice, as measured by qRT-PCR. mean ± s.e.m, $n = 6$ animals per group, * $P < 0.05$ vs WT group, # $P < 0.05$ vs Tg+NC. (E) EM examination of hippocampal neurons (CA1 domain) of Tg mice treated by intravenous injection of LNA-anti-*miR-1*. Scale bar: 2μm. (F) Derepression of TPPP/p25 protein expression in Tg mice treated with LNA-anti-*miR-1*. $n = 6$ animals per group, * $P < 0.05$ vs WT+NC, # $P < 0.05$ vs Tg+NC, mean ± s.e.m. (G) Stereotaxic injection of lenti-pre-AMO-*miR-1* into the hippocampus did not affect the decreased ejection fraction (EF %) in Tg mice. Mean ± s.e.m, $n = 6$, * $P < 0.05$. (H-J) *miR-1* levels in the heart (H), blood (I) and hippocampus (J) in *miR-1* Tg mice after stereotaxic injection of lenti-AMO-pre-*miR-1* into the CA1 of hippocampus as measured by qRT-PCR. Mean ± s.e.m, $n = 6$ animals per group, * $P < 0.05$ vs WT group, # $P < 0.05$ vs Tg+NC. (K) Stereotaxic injection of lenti-AMO-pre-*miR-1* into the hippocampus alleviates hippocampal microtubule dissolution in Tg mice at an age of 6 months, as examined via EM (Scale bar: 4μm). (L) Stereotaxic injection of lenti-AMO-pre-*miR-1* into the hippocampus enhances the expression of TPPP/p25 protein in Tg mice at an age of 6 months, as evaluated by western blot. * $P <$

0.05 vs WT; $^{\#}P < 0.05$ vs, Tg+NC; means \pm s.e.m, $n = 6$ animals per group.

Figure 7 NRVCs hypoxia induces elevation of *miR-1* in co-cultured NRNs. (A)

Experimental design: The NRVCs were seeded in the top compartment, and NRNs were cultured in the bottom compartment. A membrane with a 0.4- μ m pore size separated the two compartments to prevent NRVCs from directly connecting to the NRNs. After co-culture for 48 h with 1% O₂, the total RNA was harvested for qRT-PCR. (B, C) *miR-1* levels in NRVCs and NRNs (B) as well as the co-culture medium (C). $n = 6$ batches for NRVCs and NRNs, $n = 10$ batches for culture medium. $*P < 0.05$ vs Ctl. (D) Experimental design: The NRVCs were first cultured with 1% O₂ 12 h or 24 h. After carefully washing with PBS, NRVCs were seeded in the top compartment, and NRNs were cultured in the bottom compartment. A membrane with a 0.4- μ m pore size separated the two compartments to prevent NRVCs from directly connecting to NRNs. After co-culture 24 or 48 h with normal O₂, the total RNA was harvested for qRT-PCR. (E-F) *miR-1* levels in co-culture medium (E) as well as NRVCs and NRNs (F) after co-culture 48 h. $n = 10$ batches for NRVCs and NRNs, $n = 14$ batches for culture medium. $*P < 0.05$ vs Ctl. (G) *miR-1* levels in hypoxic NRVCs before co-culture with NRNs. $n = 11$ batches of cells for each group. $*P < 0.05$ vs Ctl. (H, I) *miR-1* levels in NRVCs (H) and NRNs (I) after co-culture with normal O₂ 24 h and 48 h. $n = 6$ batches of cells for each group. $*P < 0.05$ vs Ctl.

Figure 8 GW4869 prevents *miR-1* increases in the hippocampi of *miR-1* Tg mice and LCA mice. (A)

GW4869 inhibits CD63 expression in the cytoplasm of cardiomyocytes of Tg mice. CD63 was marked by green colour, β -actin by red colour and DAPI by blue colour. A1-A3 are longitudinal section images, and A4-A6 are transverse section images. $n = 3$. (B-D) *miR-1* levels in the hearts (B), blood (C) and hippocampus (D) after Tg mice were treated by GW4869. $n = 6$. $*P < 0.05$ vs Tg. (E) GW4869 prevents the decrease in TPPP/p25 protein expression in Tg mice. $n = 6$. $*P < 0.05$ vs Tg. (F) GW4869 inhibits CD63 expression in the cytoplasm of cardiomyocytes of MI mice. CD63 was marked by green colour, β -actin by red

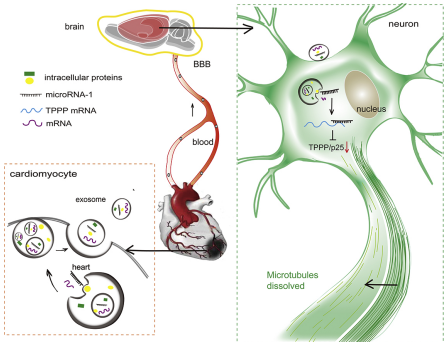
colour and DAPI by blue colour. (G) GW4869 inhibits the increased number of exosomes in the plasma of LCA mice. $n = 6$, * $P < 0.05$ vs LCA. (H,I) *miR-1* levels in the blood (H) and hippocampus (I) after LCA mice were treated by GW4869. $n = 6$, * $P < 0.05$ vs LCA. (E) GW4869 prevents the decrease in TPPP/p25 protein expression in LCA mice. $n = 6$. * $P < 0.05$ vs LCA.

Figure 9 Model for the mechanism of MI induced neuronal microtubules damage. MI induces overexpression of *miR-1* in the heart that were subsequently released into circulation and transported to the hippocampus by the help of exosomes. After fusion of exosomes and neuron, *miR-1* were released into the neuron and inhibits the expression of TPPP/p25 by binding with the 3'UTR of *TPPP/p25* gene, which further results in the microtubules dissolution.

Graphical Abstract

Highlight

- Myocardial infarction leads to *miR-1* overexpression in hippocampus.
- Exosome transports *miR-1* from the heart to brain.
- Myocardial infarction induces neuronal microtubule damage in hippocampus.
- *miR-1* results neuronal microtubule damage by downregulating TPPP/p25 protein.



Graphics Abstract

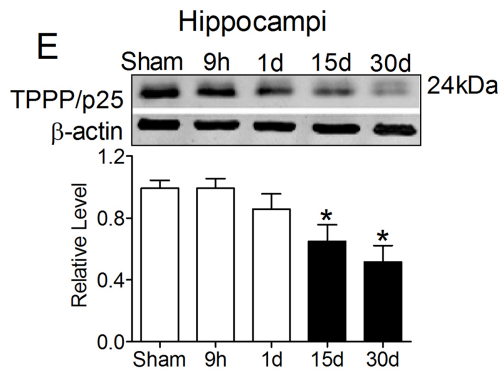
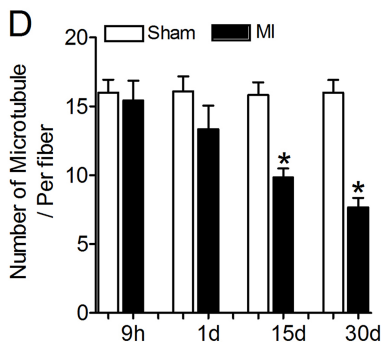
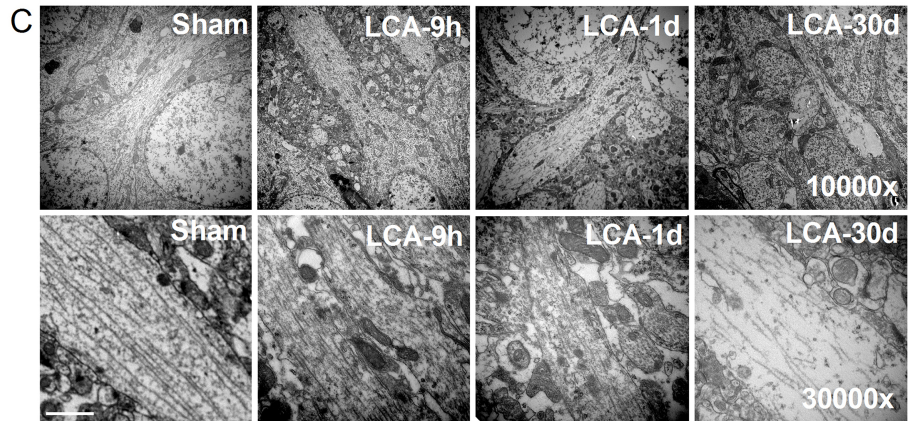
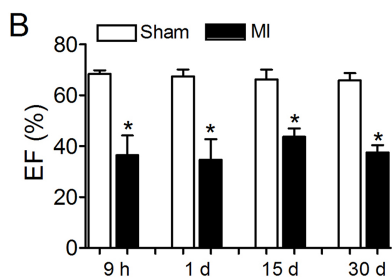
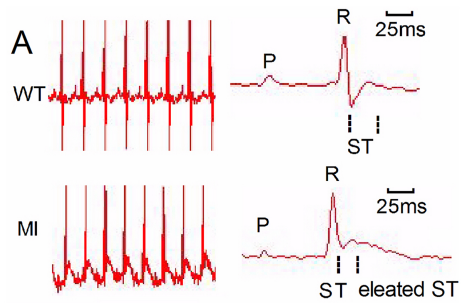
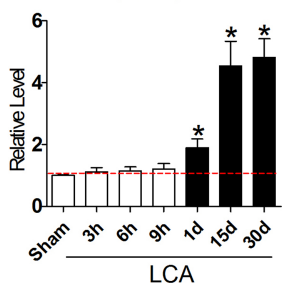


Figure 1

A Hippocampi (*miR-1*)



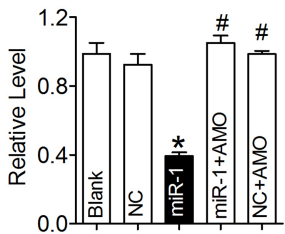
B Position 68-74 of *TPPP/p25* 3' UTR



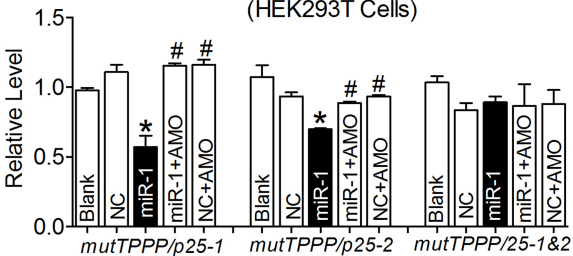
Position 1880-1886 of *TPPP/p25* 3' UTR



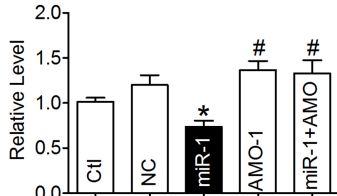
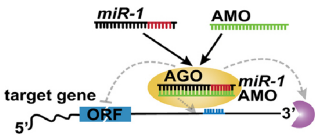
C Luciferase-Assay Wild type-*TPPP/p25* (HEK293T Cells)



D Luciferase-Assay Mut*TPPP/p25* (HEK293T Cells)



E Western blot (NRNs)



F Western Blot (NRNs)

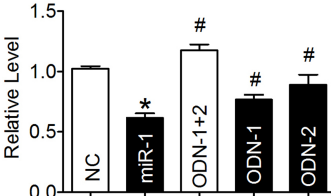
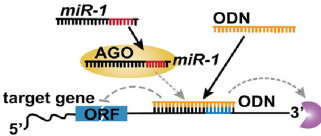


Figure 2

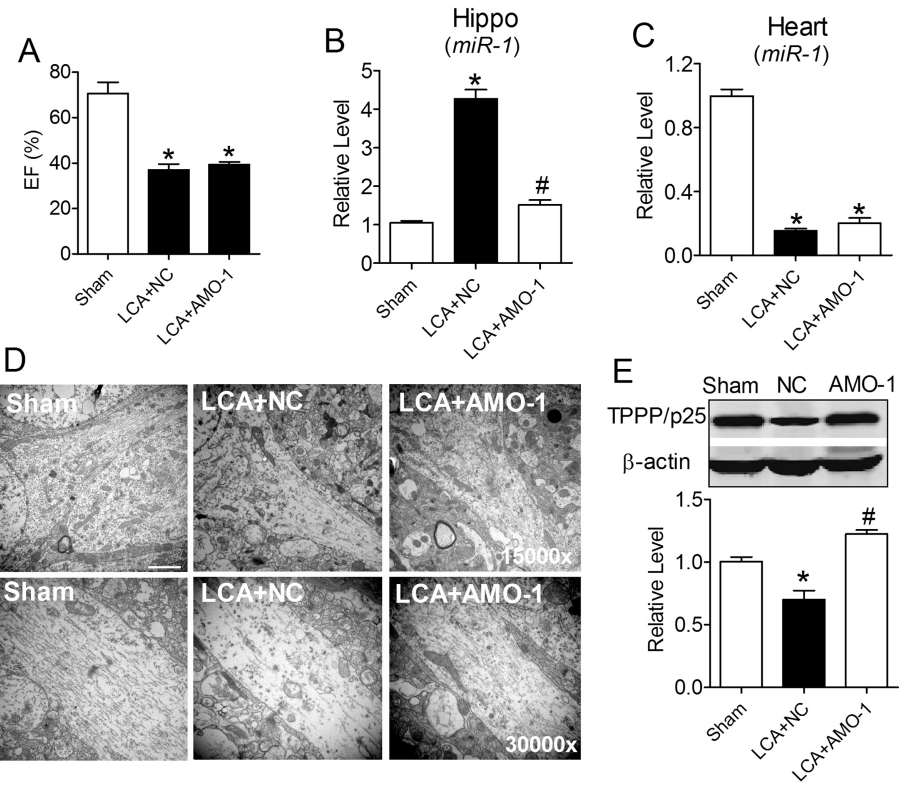


Figure 3

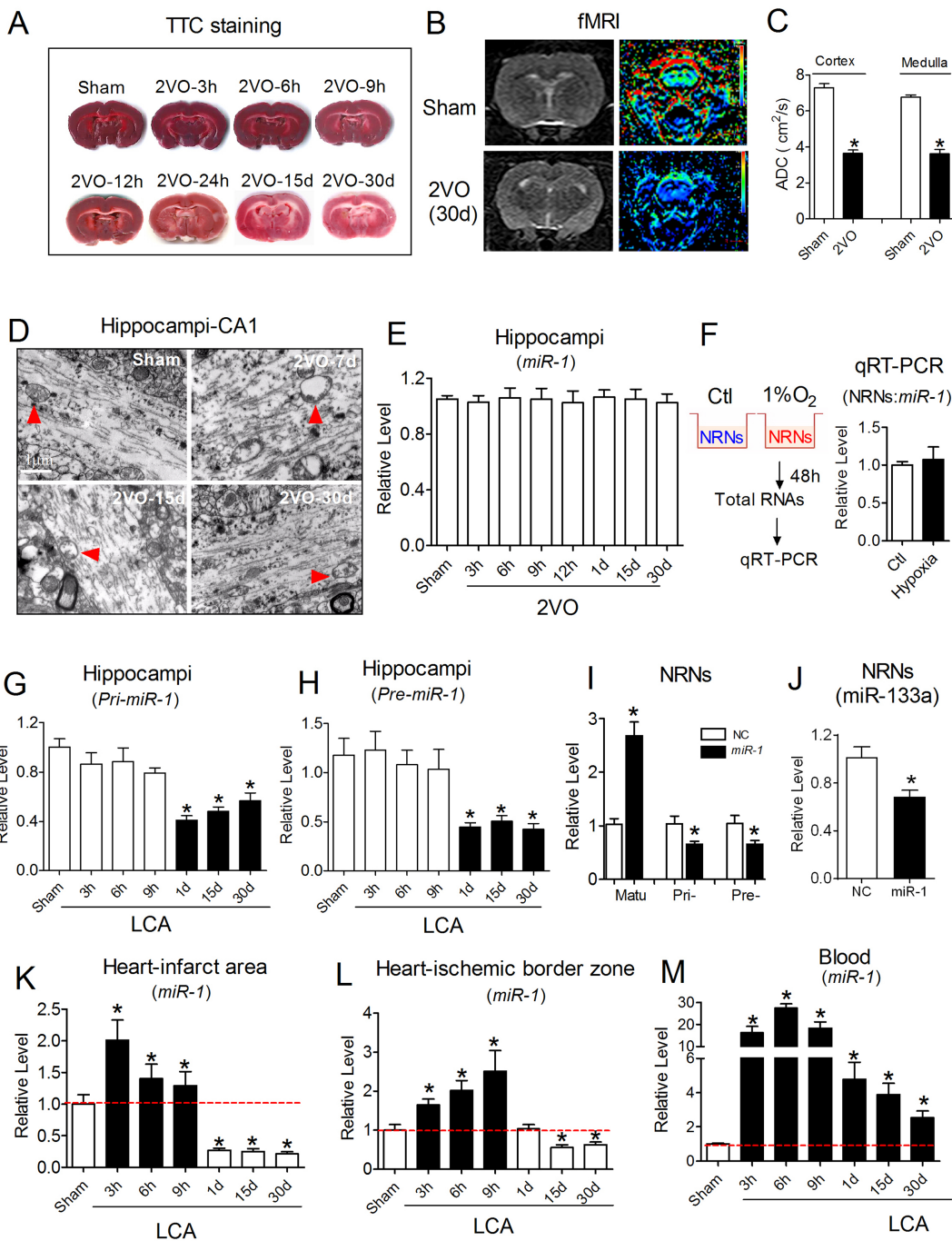


Figure 4

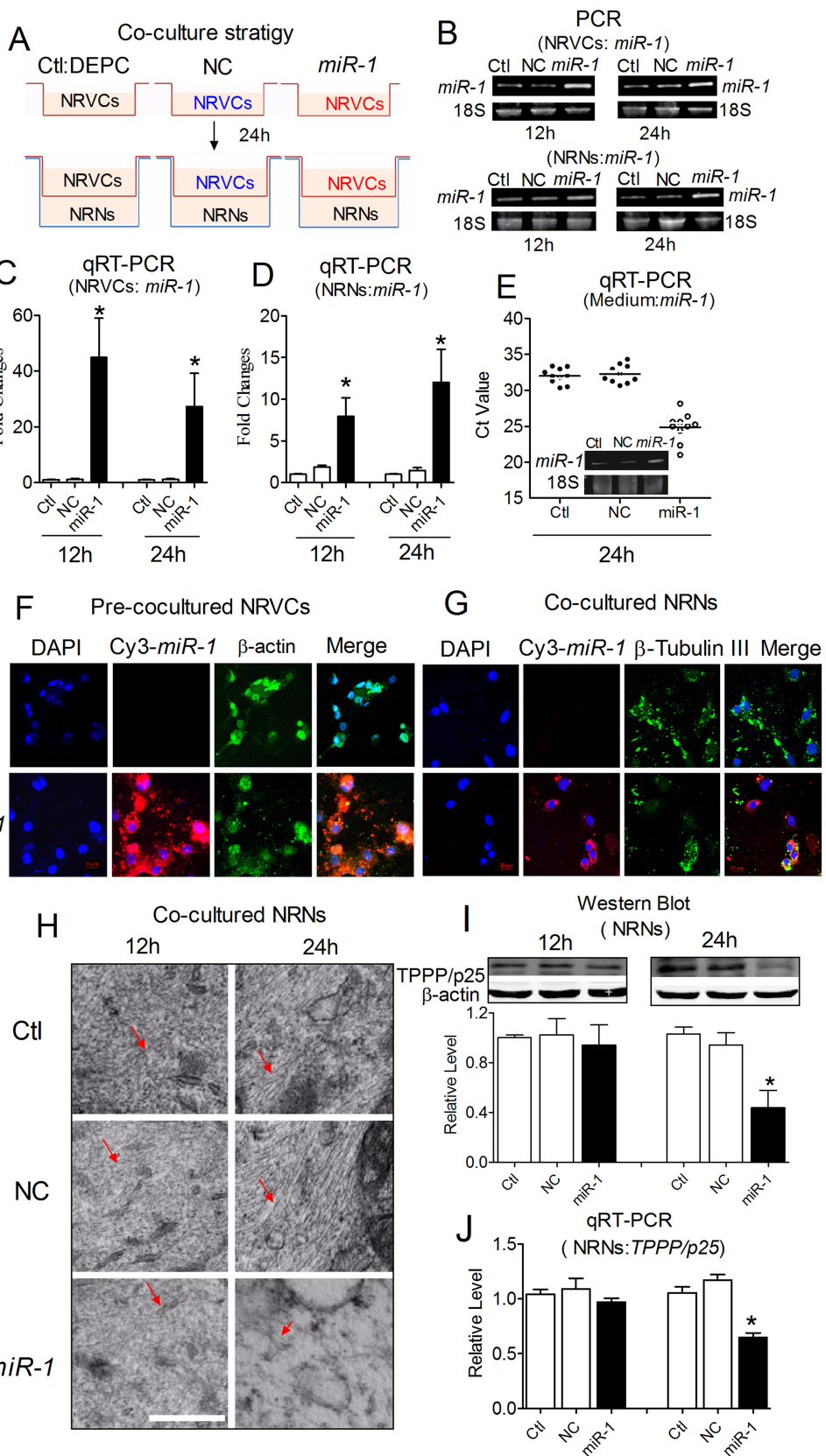


Figure 5

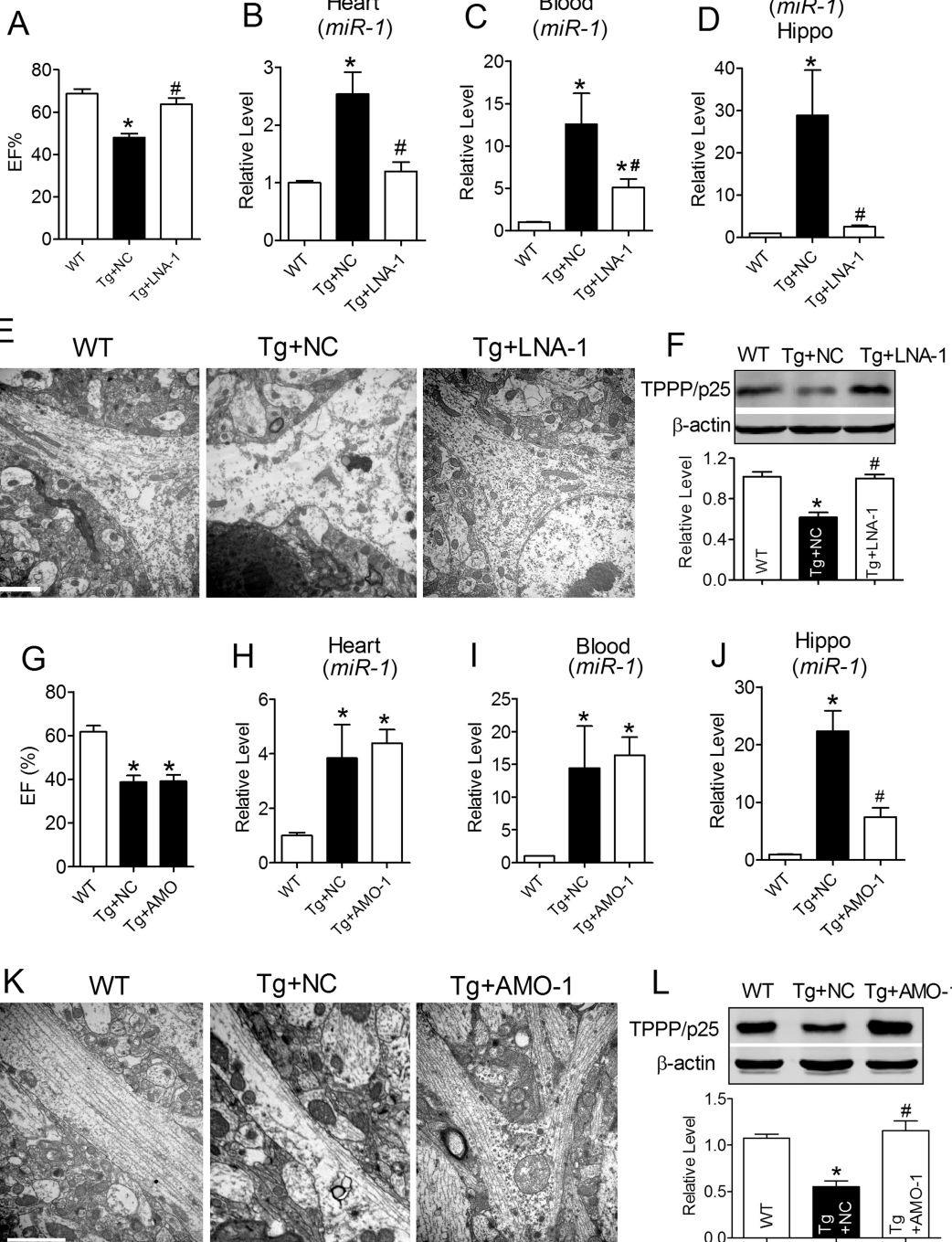


Figure 6

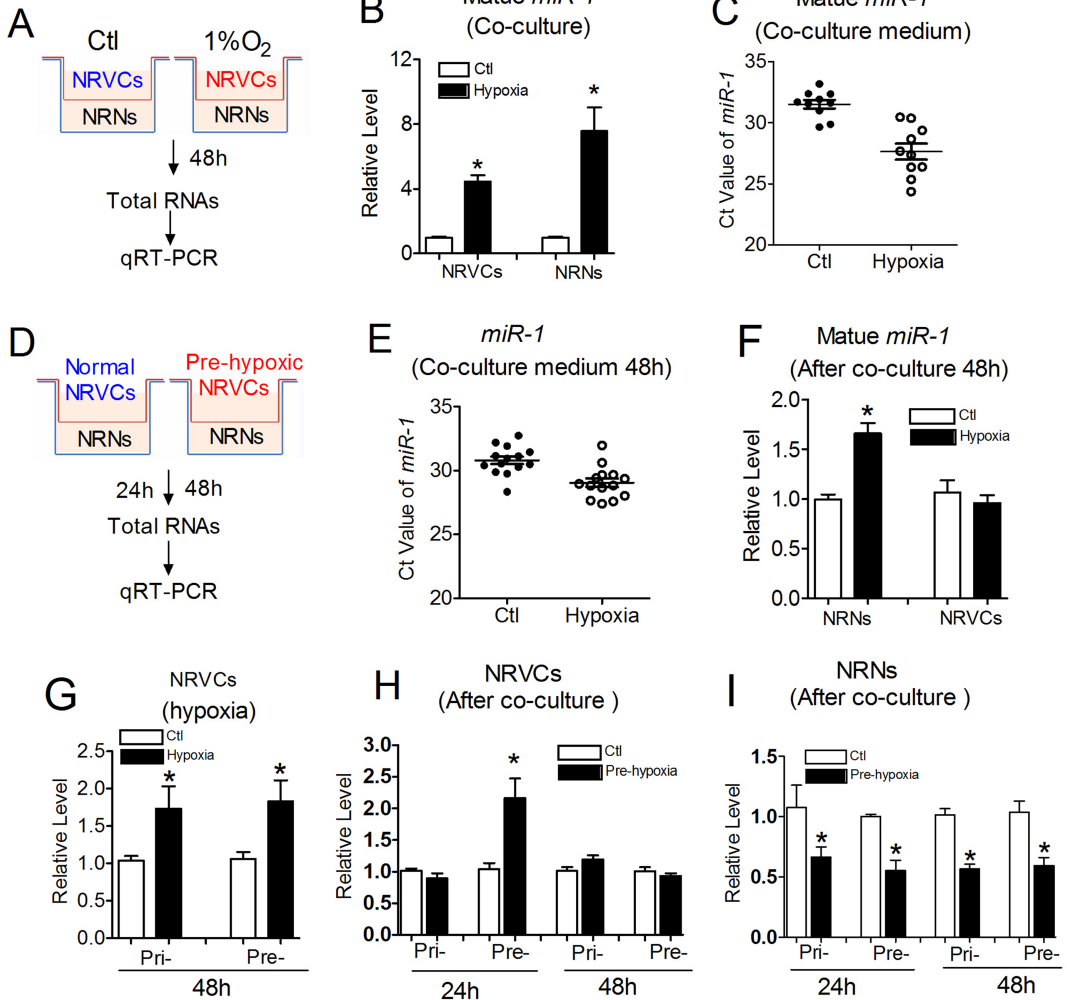


Figure 7

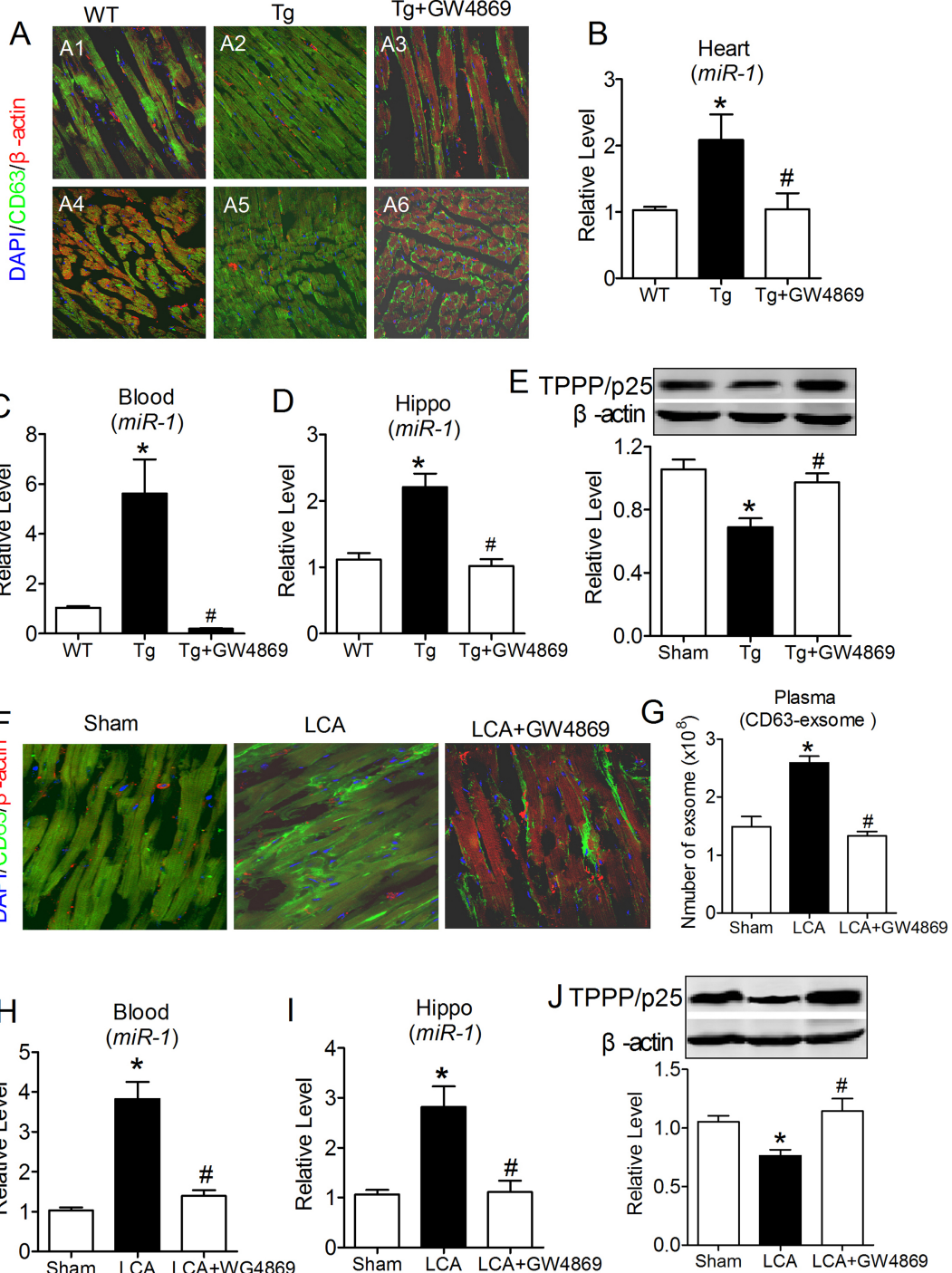


Figure 8

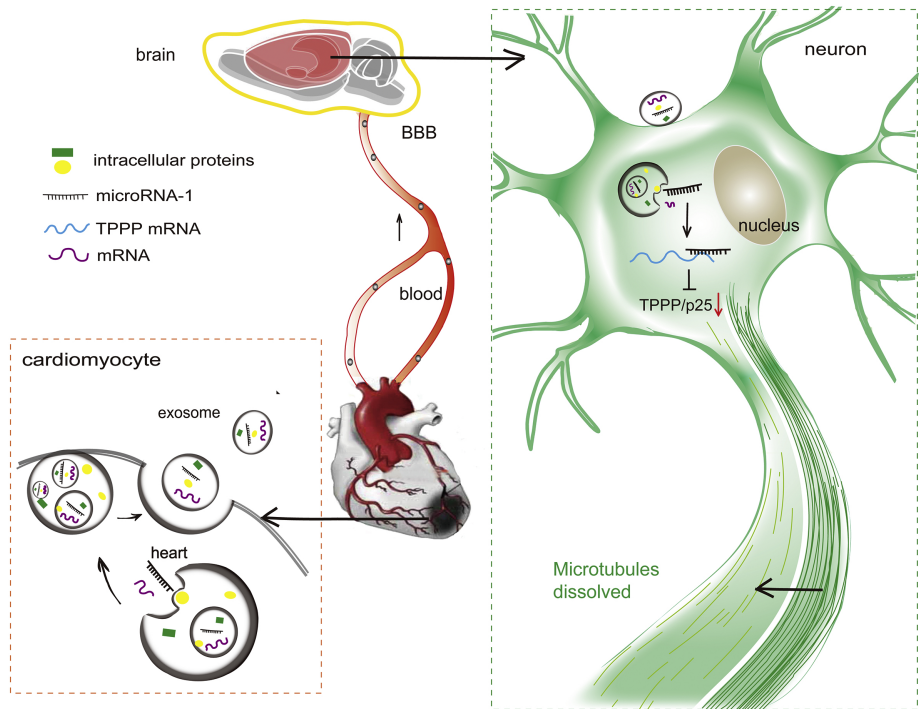


Figure 9